Letter

# Variability in marsh migration potential determined by topographic rather than anthropogenic constraints in the Chesapeake Bay region

Short title: Variability in marsh migration potential

**Grace D. Molino[1]*, Joel A. Carr[2], Neil K. Ganju[3], Matthew L. Kirwan[1]**

[1]Virginia Institute of Marine Science, William & Mary, Gloucester Point, VA, United States
[2]U.S. Geological Survey, Eastern Ecological Science Center, Beltsville, MD, United States
[3]U.S. Geological Survey, Woods Hole Coastal and Marine Science Center, Woods Hole, MA, United States

*Corresponding author:
Grace D. Molino
gdmolino@vims.edu

**Author Contribution Statement:**
MLK conceived the initial concept. GDM performed the research and conducted all analyses, and wrote the first draft of the manuscript. JAC and NKG secured funding and contributed methods. All authors contributed to manuscript writing.

**Scientific Significance Statement**

Tidal marsh migration into displaced inland ecosystems could potentially allow marshes to survive sea level rise, but it remains unknown how spatial gradients in land use and topography will limit ecosystem migration. We use high resolution mapping to demonstrate that future marsh migration area will greatly exceed historical observations and likely compensate for near complete tidal marsh area loss in the Chesapeake Bay region, United States. However, in contrast to previous work that emphasizes anthropogenic constraints, our work suggests that topography rather than land use drives spatial heterogeneity in local coastal responses along the predominantly rural U.S. coast. Future global marsh extent likely depends on migration into rural (forested, agricultural) portions of North American coasts as more developed coasts elsewhere limit marsh resilience.

**Data Availability Statement:**

Data are available in the Environmental Data Initiative repository at https://doi.org/10.6073/pasta/d57c49f666bd8b7ad692a5230573e020.

**Abstract**

Sea level rise (SLR) and saltwater intrusion are driving inland shifts in coastal ecosystems. Here, we make high-resolution (1 m) predictions of land conversion under future SLR scenarios in 81 watersheds surrounding Chesapeake Bay, United States, a hotspot for accelerated SLR and saltwater intrusion. We find that 1050-3748 $km^2$ of marsh could be created by 2100, largely at the expense of forested wetlands. Predicted marsh migration exceeds total current tidal marsh area and is ~4x greater than historical observations. Anthropogenic land use in marsh migration areas is concentrated within a few watersheds and minimally impacts calculated metrics of marsh resilience. Despite regional marsh area maintenance, local ecosystem service replacement within vulnerable watersheds remains uncertain. However, our work suggests that topography rather than land use drives spatial variability in wetland vulnerability regionally, and that rural land conversion is needed to compensate for extensive areal losses on heavily developed coasts globally.

**Key words:**

Saltwater intrusion, forested wetlands, tidal wetlands, marsh vulnerability, land use, Chesapeake Bay

## Introduction

Global climate change is leading to permanent, directional shifts in ecotones along abiotic gradients (Osland et al. 2013; Smith and Goetz 2021). Salt marshes, tidal forests, and mangroves, are all migrating landward at increasing rates, driven largely by SLR and associated increases in salinity (White and Kaplan 2017; Yao and Liu 2017). However, it remains uncertain whether this migration can occur fast enough for ecosystems to persist in the face of climate

88 change, and whether transgression can occur as ecosystems migrate into developed portions of
89 the coast (Haasnoot et al. 2021).

90 The predicted response of coastal wetlands to SLR is hotly debated (Törnqvist et al.
91 2021). Geologic reconstructions suggest a tipping point in SLR rates, after which extensive
92 drowning will occur (Horton et al. 2018; Saintilan et al. 2020). Yet numerical models suggest
93 wetlands could expand with accelerated SLR by migrating inland (Kirwan et al. 2016; Schuerch
94 et al. 2018). Saltwater intrusion inhibits germination and kills saplings of wetland tree species
95 which have low salinity tolerance, allowing for tidal marsh replacement as mature trees die
96 during extreme events (Williams et al. 1999). Forest mortality and marsh migration are well
97 documented along the North American Atlantic and Gulf coasts (Smith 2013; Kirwan and Gedan
98 2019; White et al. 2021), compensating for loss of existing tidal marsh in several regions (Raabe
99 and Stumpf 2016; Schieder et al. 2018).

100 However, the ability of marshes to migrate into adjacent upland and freshwater
101 ecosystems may be limited by steep uplands and anthropogenic barriers, resulting in "coastal
102 squeeze" (Enwright et al. 2016; Flester and Blum 2020). Less than 10% of low-lying areas on the
103 U.S. Atlantic coast have been set aside for conservation (Titus et al. 2009); and future
104 urbanization may further limit migration as available uplands become developed (Enwright et al.
105 2016). Yet low-lying, salinized agricultural land is already being abandoned (Gedan and
106 Fernández-Pascual 2019). Therefore, it remains uncertain whether marsh migration can
107 compensate for predicted marsh loss, and how natural and anthropogenic barriers may limit
108 transgression. Our work combines marsh-forest boundary delineations (Molino et al. 2021) with
109 regional land use at a higher resolution than previous studies (Holmquist et al. 2021) to uniquely

predict that salinization of uplands can maintain marsh area regionally, although functional compensation remains uncertain.

## Methods

*Study region*

We quantified potential marsh migration area (i.e., sea-level driven conversion of upland to marsh) in the low elevation region surrounding Chesapeake Bay and its tributary rivers. The Chesapeake Bay is the largest estuary in the United States, and its mixture of forested, agricultural, and developed land uses are broadly representative of the North American coastal plain. Like the U.S. coast as a whole, the upland land types most at risk from SLR are non-tidal wetlands, including palustrine emergent, forested, and scrub/shrub wetlands (Epanchin-Niell et al. 2017; Holmquist et al. 2021). Urban-dominated watersheds comprise a small fraction of the U.S. coast vulnerable to SLR (Holmquist et al. 2021). Nevertheless, the largely rural Chesapeake region includes substantial pockets of dense development (i.e., Hampton Roads, Virginia), and the regional population at risk from SLR ranks 5$^{th}$ in the U.S. (Hauer et al. 2016).

Marsh migration is well documented in Chesapeake Bay (Hussein 2009; Gedan et al. 2020). Approximately 400 km$^2$ of uplands have converted to tidal marsh over the past 150 years (Schieder et al. 2018) and rates of marsh migration are accelerating (Schieder and Kirwan 2019), driven by inundation of the low-lying gently sloping coastal-plain by relative SLR 2-3x the global average (Engelhart et al. 2009). However, marshes in this region are vulnerable to drowning due to low sediment input, microtidal tides, and accelerating rates of SLR (Stevenson et al. 1985; Kearney et al. 2002; Schepers et al. 2017). As a result, migration is a primary

mechanism of tidal marsh survival in Chesapeake Bay, making this region a model system to determine if upland conversion can compensate for loss.

*Analytical Methods*

We quantified migration of the current tidal marsh-forest boundary with SLR to estimate potential marsh migration area for the entire Chesapeake Bay coastal-plain, following a general approach established for the U.S. Gulf coast (Enwright et al. 2016). In ArcMap 10.7, we started with a previously delineated tidal marsh-forest boundary dataset of >200,000 points at 30-m resolution (Molino et al. 2020,2021). We then extracted the elevation of each point from the U.S. Geological Survey (USGS) Coastal National Elevation Database (CoNED) Topobathymetric Digital Elevation Model (Danielson and Tyler 2016). Inaccurate points were eliminated to minimize error associated with misrepresentation of the marsh-forest boundary and locations with poor elevation data (Supplemental Information). We calculated the median elevation of the tidal marsh-forest transition boundary, hereafter referred to as the threshold elevation, for USGS HUC10 (Hydrologic Unit) watersheds (USGS 2020) to account for spatial variability in processes that likely influence threshold elevation (e.g. tidal range, salinity) and quantify marsh migration at the watershed scale (Supplemental Figure 1).

Increments of SLR were added to the transition threshold elevation of each watershed to quantify potential marsh migration area, using National Oceanic and Atmospheric Administration (NOAA) global Low (0.45 m), Intermediate (1.22 m), and High (2.66 m) scenarios adjusted for the Chesapeake Bay region (Sweet et al. 2017). Land between the threshold elevation and the threshold elevation plus the SLR scenario was considered to be potential marsh migration area. Following previous approaches, we neglect accretional and

155 erosional processes that affect the longevity of converted tidal marsh area (Enwright et al. 2016;
156 Borchert et al. 2018; Holmquist et al. 2021). Thus, our estimates of potential marsh migration
157 area should not be considered predictions of long-term marsh extent, as future marsh extent
158 would be vulnerable to losses at the seaward edge (Törnqvist et al. 2021).

159 We assume that transition threshold elevations determined from the marsh-forest
160 boundary are representative of marsh-upland boundaries in general given that forested uplands
161 comprise more than half of total upland land use, and that other upland land uses (e.g.
162 agriculture), are typically separated from wetlands by a forested buffer. Preliminary observations
163 suggest that threshold elevations for non-forested boundaries are similar to the elevations of the
164 marsh-forest boundary (Supplemental Table 1). However, more work is needed to refine this
165 method for other land uses. We also assume that migration is not limited by hydrological
166 connectivity (Poulter and Halpin 2008), or highly localized freshwater inputs that cannot be
167 inferred at the scale of HUC10 watersheds. Future work that includes hydrodynamic modeling
168 could resolve these predictions at even finer spatial scales.

169 Following Gesch (2012), we calculated uncertainty envelopes for area converted under
170 the localized NOAA predictions by adding and subtracting the RMSE of CoNED (20 cm) from
171 the new marsh-upland elevation within each watershed (Danielson and Tyler, 2016). Current
172 marsh area was determined from the National Wetlands Inventory (NWI) (U.S. Fish and Wildlife
173 Service 2018). The current land use of predicted marsh migration areas was assessed using the
174 Chesapeake Conservancy High Resolution Land Use and Land Cover datasets (Chesapeake
175 Conservancy 2018a;b) for six categories: forest, forested wetlands, turf grass, agriculture,
176 impervious, and other (Supplemental Table 2). Forested wetlands were included separately from
177 the forest category because their physiographic position results in a higher sensitivity to flooding

178 and salinity stresses (Doyle et al. 2007). The “other” category includes mixed open and mixed
179 impervious as well as marsh located at elevations above the median threshold value for each
180 watershed.
181
182 **Results**
183 Median tidal marsh-forest boundary elevations were determined for 81 watersheds from a
184 final dataset of 95,286 points. The median threshold elevation of transition from tidal marsh to
185 forest around Chesapeake Bay is 0.54 m NAVD88. Median threshold elevations for HUC10
186 watersheds range from 0.20 m NAVD88 in the southernmost watersheds, to 1.05 m NAVD88
187 along the Atlantic coastal lagoons (Figure 1). Unique land conversion estimates for each
188 watershed (Supplemental Table 3) were combined to produce an estimate of potential upland
189 conversion for the entire Chesapeake Bay coastal-plain (Figure 2). Extensive areas of land
190 conversion are predicted along the main stem of Chesapeake Bay (Figure 2B,D), with limited
191 migration along the western shore tributaries and in the Atlantic coastal lagoons at each SLR
192 scenario (Figure 2A,C) (Molino et al. 2022).
193 Marsh migration area increased through time and with the magnitude of SLR, ranging
194 from 1050 $km^2$ (NOAA Low) to 3748 $km^2$ (NOAA High) by 2100 (Figure 3A;Supplemental
195 Table 4) and is currently dominated by terrestrial and wetland forests. Developed land uses,
196 including agriculture and impervious surfaces, generally occupy less than 10% of predicted
197 migration areas in individual watersheds, despite more extensive development in watersheds
198 overall (Figure 3B;Supplemental Table 5). For example, Elizabeth River surrounding Norfolk,
199 VA is one of the most developed watersheds in the Chesapeake Bay and the U.S., but impervious

surfaces occupy only 16% of potential marsh migration area under 1 m of SLR, compared to 31% for the entire watershed (Supplemental Table 6).

## Discussion

### *Quantifying elevation thresholds*

Predictions of coastal ecosystem migration typically depend on establishing threshold elevations, beyond which inundation drives state change (Enwright et al. 2016; Borchert et al. 2018; Mitchell et al. 2020). A single threshold elevation is often determined for large areas (e.g. county, estuary) despite potential spatial variation in the processes that control threshold elevation. For example, the elevation range of vegetated tidal marsh in Chesapeake Bay is thought to be controlled by tidal range, weather events, and salinity, where marshes exposed to greater water level fluctuations and higher salinities tend to have higher threshold elevations (Boon et al. 1977). Alternatively, previous modeling and remote sensing studies of marsh vulnerability typically assume that the upper elevation limit of marsh corresponds to astronomical tidal datums alone (e.g. highest astronomical tide (HAT)) (Thorne et al. 2018; Mitchell et al. 2020; Holmquist et al. 2021). However, we demonstrate that salinity is also a driver of threshold elevation (Figure 1B;Supplemental Figure 2). Our study relies on tidal marsh-forest boundaries determined independently from these metrics (Molino et al. 2021), allowing us to capture small-scale variability from both tidal range and salinity, despite a large study area. Our median threshold elevation (0.54 m) determined across the entire Chesapeake Bay from aerial imagery is largely in agreement with the threshold elevation determined from mean HAT in Virginia (0.61 m) (Mitchell et al. 2020). However, we find that threshold elevations vary more than 5-fold across our study region, from 0.20 m NAVD88 in low salinity watersheds to 1.05 m

NAVD88 in exposed, high salinity watersheds (Figure 1;St-Laurent et al. 2020). These results suggest that using a single threshold elevation for large sections of the coast could result in significant under- or over-estimations of future marsh migration at smaller spatial scales and precludes attempts to account for spatial variability in wetland vulnerability.

*Natural and anthropogenic barriers to marsh migration*

Steep topography and anthropogenic land uses are well-known barriers to marsh migration (Torio and Chmura 2013; Enwright et al. 2016). We found extensive marsh migration predicted in the gently sloping watersheds of the Eastern Shore of Chesapeake Bay, and more limited marsh migration predicted in watersheds with steep topography along the western shore tributaries and Atlantic coast (Figure 4B). These finding are consistent with observations of rapid forest retreat in other low slope portions of the Atlantic coastal plain (Smith 2013; Schieder and Kirwan 2019; Ury et al. 2021), and the conceptual understanding that topography constrains marsh migration (Kirwan et al. 2016; Mitchell et al. 2017). Moreover, these findings suggest that although marsh migration will be extensive in Chesapeake Bay, natural topographic variability will lead to substantial gradients in potential marsh migration and vulnerability to SLR.

Anthropogenic land uses also potentially limit upland conversion into marsh, especially in regions of the world with large urban centers and extensive agriculture (Schuerch et al. 2018). Like the U.S. coast as a whole, the Chesapeake Bay region is largely rural with pockets of intensive development (Holmquist et al. 2021). Our high-resolution, spatially-explicit approach allows us to take advantage of that heterogeneity and evaluate specific land use limitations by examining responses in watersheds with major urban centers and agricultural land use. We found that developed land use (impervious + agricultural) within low elevation areas most vulnerable to

246 marsh migration (i.e., land <1.0 m above current threshold elevations) was concentrated within a
247 minority of watersheds and was usually dominated by one developed land use class (Figure 4).
248 Regionally, impervious land use in potential marsh migration areas was minimal through high
249 SLR scenarios (Figure 3B). For example, three of the five major urban centers in our study
250 region (Hampton, VA; Annapolis, MD; Baltimore, MD) are located in watersheds with only
251 small areas of potential marsh migration. Two urban centers (Norfolk and Newport News, VA)
252 were located in watersheds with moderate marsh migration, but impervious cover only accounted
253 for 14-16% of predicted marsh migration area despite extensive development inland. Despite the
254 perception that major urban centers will heavily limit marsh migration, our high-resolution
255 predictions suggest that the most vulnerable land in the Chesapeake Bay remains largely
256 undeveloped, even in urban watersheds with extensive development.
257 Agricultural land use was more widespread in watersheds with extensive predicted marsh
258 migration area and dominated developed land use. Agricultural land exceeded 10% of predicted
259 marsh migration area in twenty-three watersheds whereas impervious land cover exceeded 10%
260 in only nine watersheds (Supplemental Table 6). Recent abandonment of agricultural fields with
261 saltwater intrusion is being documented (Gedan et al. 2020). The majority of future marsh
262 migration area under 1.0 m of SLR is predicted to come at the expense of freshwater forested
263 ecosystems (870 $km^2$; Figure 3B), which are more prevalent than developed land in low-lying
264 areas in 78 of 81 watersheds (Supplemental Table 7). Together, these observations suggest that
265 highly variable land use across the broader Chesapeake region has relatively small influence on
266 regional marsh migration, and that gradients in topography rather than anthropogenic land uses
267 are the primary influence on spatial variability of marsh migration potential.
268

*Implications for marsh vulnerability*

Coastal wetlands are threatened by global SLR and declining riverine sediment yields to the coast (Syvitski et al. 2005; Törnqvist et al. 2021). Predictions of wetland fate range from place-based estimates of loss (Crosby et al. 2016; Mitchell et al. 2020) to generalized models of expansion (Kirwan et al. 2016; Schuerch et al. 2018), depending largely on the ability of wetlands to migrate inland at rates faster than existing wetlands convert to open water. Our work shows unequivocally that future land conversion will be extensive in the Chesapeake Bay region. Across the entire Chesapeake Bay, we predict that 1050-3748 $km^2$ of new marshes will potentially be created by 2100 (Figure 3A). Thus, predictions of potential marsh migration area over the next 80 years are approximately 2-9x greater than that inferred from historical maps over the last 150 years (400 $km^2$; Schieder et al. 2018). Moreover, predicted marsh migration area under Low to Intermediate SLR scenarios is similar to the current total area of marshes today (1454 $km^2$), and is more than twice the current tidal marsh area under faster scenarios (Figure 3). These predictions of extensive land conversion suggest that, at the scale of the entire Chesapeake Bay, marsh migration could compensate for tidal marsh area loss under most SLR scenarios, even if all existing marshes drowned or were lost to erosion.

Marsh resilience is controlled by the interplay between vertical and lateral ecosystem vulnerabilities (Ganju et al. 2017; Fitzgerald and Hughes 2019). Following Holmquist et al. 2021, we estimate a marsh lateral resilience index as the ratio between marsh migration area under 1.0 m of SLR and current tidal marsh area for each watershed. Watersheds with ratios >1 are considered resilient to SLR as inland migration could compensate for even a complete loss of existing marshes. Conversely, watersheds with ratios <1 are considered potentially vulnerable. We found substantial spatial variability in lateral marsh resilience (Figure 5) largely attributable

to geomorphological differences throughout the region. For example, watersheds comprising the Atlantic coastal lagoons are vulnerable because extensive tidal marshes today are bounded by relatively steep adjacent topography (Figure 5A). Watersheds along Mobjack Bay (Figure 2D) are considered resilient as the low-lying area predicted to be inundated with 1.0 m of SLR is more than double current tidal marsh area (Figure 5A). Interestingly, the watershed with the largest tidal marshes and most extensive marsh loss (i.e., Blackwater River) (Kearney et al. 2002; Schepers et al. 2017) is only moderately vulnerable to SLR because migration areas are large enough to compensate for a near complete loss of existing tidal marsh (ratio 0.90).

Landowners may perceive marsh migration negatively, and may attempt to defend developed land uses from SLR (Field et al. 2017; Van Dolah et al. 2020). Interestingly, we find that lateral tidal marsh vulnerability increased only slightly when anthropogenic land uses were completely removed from the marsh migration area: (i.e., only two watersheds shift from resilient to vulnerable) (Figure 5B). Six of the eight most developed watersheds have a resilience index greater than one, and the remaining two watersheds have a resilience index of less than one with or without including developed land in the migration area (Supplemental Table 5;Figure 5B). In contrast, tidal marsh vulnerability is very sensitive to the inclusion of freshwater forested ecosystem area (Supplemental Table 6;Figure 5C). Thus, our work points to extensive marsh migration regardless of land use, though tidal marsh resilience comes at the expense of forests and forested wetlands.

The largescale conversion of forests and forested wetlands to tidal marsh has significant implications for ecosystem function. Salinization of forested wetlands could exacerbates coastal eutrophication (Noe et al. 2013) and loss of critical habitat for avian species (Brittain and Craft 2012). While marsh carbon burial rates surpass that of coastal forests, extensive time to

315 replacement could limit carbon sequestration compensation (Smith and Kirwan 2021). Moreover,
316 migrating marshes are typically dominated by invasive *Phragmites australis* rather than native
317 wetland species (Smith 2013; Langston et al. 2021), making functional compensation uncertain
318 despite areal maintenance. Future work could help to better distinguish between forest and
319 forested wetlands in remotely sensed imagery, and to quantify potential loss of ecosystem
320 services.

321 Previous work at a variety of scales emphasized the spatial heterogeneity of coastal
322 responses to SLR and saltwater intrusion (Pendleton et al. 2010; Lentz et al. 2016). More
323 specifically, tidal marshes along gently sloping, natural coastlines are considered more resilient
324 to SLR than marshes along steep, anthropogenic-dominated coastlines (Kirwan and Megonigal
325 2013; Holmquist et al. 2021). Our approach to defining threshold elevations at the scale of
326 individual watersheds allows for a more precise assessment of spatial variability and the
327 influence of salinity. Our findings of wide variability in threshold elevations (0.20-1.05 m
328 NAVD88), marsh migration areas (<1-131 $km^2$), and lateral tidal marsh vulnerability indices
329 (0.1-106.9) are consistent with the paradigm that spatial variability in topography and land use
330 will lead to a heterogenous response. However, we uniquely find that low-lying areas are largely
331 undeveloped, even in watersheds with substantial agriculture and urbanization. Therefore, we
332 suggest that spatial gradients in forest mortality, sea-level driven land conversion, and marsh
333 vulnerability are more fundamentally related to topography than anthropogenic land use in the
334 Chesapeake Bay.

335 Strong spatial gradients in topography and land use imprinted on a largely rural landscape
336 also define the land vulnerable to SLR on the U.S. coast as a whole (Borchert et al. 2018;
337 Holmquist et al. 2021). This suggests that observations from the Chesapeake Bay may be more

broadly applicable. However, our findings that marsh migration and resilience are not overly limited by anthropogenic land use does not apply to regions of the world with higher population densities and extensive hardened shorelines (e.g. Europe, Asia) (Kabat et al. 2005; Ma et al. 2014; CIESIN 2017). Therefore, spatial gradients at the scale of individual watersheds in the Chesapeake Bay may resemble larger-scale gradients, where global marsh extent will only be maintained if marsh loss in developed portions of the world are offset by migration into more rural regions.


## Acknowledgments

This work was funded by the U.S. Geological Survey Climate Research and Development and the U.S. Geological Survey Coastal and Marine Hazards and Resources Program. Additional funding was provided from the National Science Foundation CAREER, LTER, and CZN programs (EAR-1654374, DEB-1832221, and EAR-2012670). We appreciate conversations with Molly Mitchell that improved the work. Any use of trade, firm, or product names is for descriptive purposes only and does not imply endorsement by the US Government. This is contribution number 4098 of the Virginia Institute of Marine Science.


## References


Boon, J. D., M. E. Boule, and G. M. Silberhorn. 1977. Delineation of Tidal Boundaries in Lower Chesapeake Bay and its Tributaries. Spec. Reports Appl. Mar. Sci. Ocean Eng. (SRAMSOE) No. 140. Virginia Institute of Marine Science, William & Mary. doi:10.21220/V50160

Borchert, S. M., M. J. Osland, N. M. Enwright, and K. T. Griffith. 2018. Coastal wetland adaptation to sea level rise: Quantifying potential for landward migration and coastal squeeze. J. Appl. Ecol. **55**: 2876–2887. doi:10.1111/1365-2664.13169

Brittain, R. A., and C. B. Craft. 2012. Effects of sea-level rise and anthropogenic development on priority bird species habitats in coastal Georgia, USA. Environ. Manage. **49**: 473–482. doi:10.1007/s00267-011-9761-x

Chesapeake Conservancy. 2018a. Land Use Data Project 2013/2014.

Chesapeake Conservancy. 2018b. Land Cover Data Project 2013/2014.

CIESIN - Columbia University. 2017. Gridded Population of the World, Version 4 (GPWv4): Population Count Adjusted to Match 2015 Revision of UN WPP Country Totals, Revision 10.

Crosby, S. C., D. F. Sax, M. E. Palmer, H. S. Booth, L. A. Deegan, M. D. Bertness, and H. M. Leslie. 2016. Salt marsh persistence is threatened by predicted sea-level rise. Estuar. Coast. Shelf Sci. **181**: 93–99. doi:10.1016/j.ecss.2016.08.018

Danielson, J., and D. Tyler. 2016. Topobathymetric Model for Chesapeake Bay Region - District of Columbia, States of Delaware, Maryland, Pennsylvania, and Virginia, 1859 to 2015.

Van Dolah, E. R., C. D. Miller Hesed, and M. J. Paolisso. 2020. Marsh Migration, Climate Change, and Coastal Resilience: Human Dimensions Considerations for a Fair Path Forward. Wetlands **40**: 1751–1764.

375 doi:10.1007/s13157-020-01388-0

376 Doyle, T. W., C. P. O'Neil, M. P. V. Melder, A. S. From, and M. M. Palta. 2007. Tidal freshwater swamps of the
377 Southeastern United States: Effects of land use, hurricanes, sea-level rise, and climate change, p. 1–28. *In*
378 W.H. Conner, T.W. Doyle, and K.W. Krauss [eds.], Ecology of Tidal Freshwater Forested Wetlands of the
379 Southeastern United States. Springer.

380 Engelhart, S. E., B. P. Horton, B. C. Douglas, W. R. Peltier, and T. E. Törnqvist. 2009. Spatial variability of late
381 Holocene and 20th century sea-level rise along the Atlantic coast of the United States. Geology **37**: 1115–
382 1118. doi:10.1130/G30360A.1

383 Enwright, N. M., K. T. Griffith, and M. J. Osland. 2016. Barriers to and opportunities for landward migration of
384 coastal wetlands with sea-level rise. Front. Ecol. Environ. **14**: 307–316. doi:10.1002/fee.1282

385 Epanchin-Niell, R., C. Kousky, A. Thompson, and M. Walls. 2017. Threatened protection: Sea level rise and coastal
386 protected lands of the eastern United States. Ocean Coast. Manag. **137**: 118–130.
387 doi:10.1016/j.ocecoaman.2016.12.014

388 Field, C. R., A. A. Dayer, and C. S. Elphick. 2017. Landowner behavior can determine the success of conservation
389 strategies for ecosystem migration under sea-level rise. Proc. Natl. Acad. Sci. U. S. A. **114**: 9134–9139.
390 doi:10.1073/pnas.1620319114

391 Fitzgerald, D. M., and Z. Hughes. 2019. Marsh processes and their response to climate change and sea-level rise.
392 Annu. Rev. Earth Planet. Sci. **47**: 481–517. doi:10.1146/annurev-earth-082517-010255

393 Flester, J. A., and L. K. Blum. 2020. Rates of Mainland Marsh Migration into Uplands and Seaward Edge Erosion
394 are Explained by Geomorphic Type of Salt Marsh in Virginia Coastal Lagoons. Wetlands **40**: 1703–1715.
395 doi:10.1007/s13157-020-01390-6

396 Ganju, N. K., Z. Defne, M. L. Kirwan, S. Fagherazzi, A. D'Alpaos, and L. Carniello. 2017. Spatially integrative
397 metrics reveal hidden vulnerability of microtidal salt marshes. Nat. Commun. **8**. doi:10.1038/ncomms14156

398 Gedan, K. B., R. Epanchin-Niell, and M. Qi. 2020. Rapid Land Cover Change in a Submerging Coastal County.
399 Wetlands **40**: 1717–1728. doi:10.1007/s13157-020-01328-y

400 Gedan, K. B., and E. Fernández-Pascual. 2019. Salt marsh migration into salinized agricultural fields: A novel
401 assembly of plant communities. J. Veg. Sci. **30**: 1007–1016. doi:10.1111/jvs.12774

402 Gesch, D. B. 2012. Elevation Uncertainty in Coastal Inundation Hazard Assessments, p. 121–140. *In* S. Cheval
403 [ed.], Natural Disasters. InTech.

404 Haasnoot, M., J. Lawrence, and A. K. Magnan. 2021. Pathways to coastal retreat. Science (80-. ). **372**: 1287–1290.
405 doi:10.1126/science.abi6594

406 Hauer, M. E., J. M. Evans, and D. R. Mishra. 2016. Millions projected to be at risk from sea-level rise in the
407 continental United States. Nat. Clim. Chang. **6**: 691–695. doi:10.1038/nclimate2961

408 Holmquist, J. R., L. N. Brown, and G. M. MacDonald. 2021. Localized Scenarios and Latitudinal Patterns of
409 Vertical and Lateral Resilience of Tidal Marshes to Sea-Level Rise in the Contiguous United States. Earth's
410 Futur. **9**. doi:10.1029/2020ef001804

411 Horton, B. P., I. Shennan, S. L. Bradley, N. Cahill, M. Kirwan, R. E. Kopp, and T. A. Shaw. 2018. Predicting marsh
412 vulnerability to sea-level rise using Holocene relative sea-level data. Nat. Commun. **9**. doi:10.1038/s41467-
413 018-05080-0

414 Hussein, A. H. 2009. Modeling of Sea-Level Rise and Deforestation in Submerging Coastal Ultisols of Chesapeake
415 Bay. Soil Sci. Soc. Am. J. **73**: 185–196. doi:10.2136/sssaj2006.0436

416 Kabat, P., W. van Vierssen, J. Veraart, P. Vellinga, and J. Aerts. 2005. Climate proofing the Netherlands. Nature
417 **438**: 283–284. doi:10.1038/438283a

Kearney, M. S., A. S. Rogers, J. R. G. Townshend, E. Rizzo, D. Stutzer, J. C. Stevenson, and K. Sundborg. 2002. Landsat imagery shows decline of coastal marshes in chesapeake and delaware bays. Eos (Washington. DC). **83**: 173–184. doi:10.1029/2002EO000112

Kirwan, M. L., and K. B. Gedan. 2019. Sea-level driven land conversion and the formation of ghost forests. Nat. Clim. Chang. **9**: 450–457. doi:10.1038/s41558-019-0488-7

Kirwan, M. L., and J. P. Megonigal. 2013. Tidal wetland stability in the face of human impacts and sea-level rise. Nature **504**: 53–60. doi:10.1038/nature12856

Kirwan, M. L., D. C. Walters, W. G. Reay, and J. A. Carr. 2016. Sea level driven marsh expansion in a coupled model of marsh erosion and migration. Geophys. Res. Lett. **43**: 4366–4373. doi:10.1002/2016GL068507

Langston, A. K., D. J. Coleman, N. W. Jung, and others. 2021. The Effect of Marsh Age on Ecosystem Function in a Rapidly Transgressing Marsh. Ecosystems. doi:10.1007/s10021-021-00652-6

Lentz, E. E., E. R. Thieler, N. G. Plant, S. R. Stippa, R. M. Horton, and D. B. Gesch. 2016. Evaluation of dynamic coastal response to sea-level rise modifies inundation likelihood. Nat. Clim. Chang. **6**: 696–700. doi:10.1038/nclimate2957

Ma, Z., D. S. Melville, J. Liu, and others. 2014. Rethinking China's new great wall. Science (80-. ). **346**: 912–914. doi:10.1126/science.1257258

Mitchell, M., J. Herman, D. M. Bilkovic, and C. Hershner. 2017. Marsh persistence under sea-level rise is controlled by multiple, geologically variable stressors. Ecosyst. Heal. Sustain. **3**. doi:10.1080/20964129.2017.1396009

Mitchell, M., J. Herman, and C. Hershner. 2020. Evolution of Tidal Marsh Distribution under Accelerating Sea Level Rise. Wetlands **40**: 1789–1800. doi:10.1007/s13157-020-01387-1

Molino, G. D., J. A. Carr, N. K. Ganju, and M. L. Kirwan. 2022. Spatial Variability in Marsh Vulnerability and Coastal Forest Loss in Chesapeake Bay ver 1.doi:https://doi.org/10.6073/pasta/5f67dfab12021a36aa1886604844fbaa

Molino, G. D., Z. Defne, A. L. Aretxabaleta, N. K. Ganju, and J. A. Carr. 2021. Quantifying Slopes as a Driver of Forest to Marsh Conversion Using Geospatial Techniques: Application to Chesapeake Bay Coastal-Plain, United States. Front. Environ. Sci. **9**. doi:10.3389/fenvs.2021.616319

Molino, G. D., Z. Defne, N. K. Ganju, J. A. Carr, G. R. Gutenspergen, and D. C. Walters. 2020. Slope Values Across Marsh-Forest Boundary in Chesapeake Bay Region, USA.doi:10.5066/P9EJ6PGT

Noe, G. B., K. W. Krauss, B. G. Lockaby, W. H. Conner, and C. R. Hupp. 2013. The effect of increasing salinity and forest mortality on soil nitrogen and phosphorus mineralization in tidal freshwater forested wetlands. Biogeochemistry **114**: 225–244. doi:10.1007/s10533-012-9805-1

Osland, M. J., N. Enwright, R. H. Day, and T. W. Doyle. 2013. Winter climate change and coastal wetland foundation species: Salt marshes vs. mangrove forests in the southeastern United States. Glob. Chang. Biol. **19**: 1482–1494. doi:10.1111/gcb.12126

Pendleton, E. A., E. R. Thieler, and S. J. Williams. 2010. Importance of coastal change variables in determining vulnerability to sea- and lake-level change. J. Coast. Res. **26**: 176–183. doi:10.2112/08-1102.1

Poulter, B., and P. N. Halpin. 2008. Raster modelling of coastal flooding from sea-level rise. Int. J. Geogr. Inf. Sci. **22**: 167–182. doi:10.1080/13658810701371858

Raabe, E. A., and R. P. Stumpf. 2016. Expansion of Tidal Marsh in Response to Sea-Level Rise: Gulf Coast of Florida, USA. Estuaries and Coasts **39**: 145–157. doi:10.1007/s12237-015-9974-y

Saintilan, N., N. S. Khan, E. Ashe, J. J. Kelleway, K. Rogers, C. D. Woodroffe, and B. P. Horton. 2020. Thresholds of mangrove survival under rapid sea level rise. Science (80-. ). **368**: 1118–1121. doi:10.1126/science.aba2656

Schepers, L., M. Kirwan, G. Guntenspergen, and S. Temmerman. 2017. Spatio-temporal development of vegetation

die-off in a submerging coastal marsh. Limnol. Oceanogr. **62**: 137–150. doi:10.1002/lno.10381

Schieder, N. W., and M. L. Kirwan. 2019. Sea-level driven acceleration in coastal forest retreat. Geology **47**: 1151–1155. doi:10.1130/G46607.1

Schieder, N. W., D. C. Walters, and M. L. Kirwan. 2018. Massive Upland to Wetland Conversion Compensated for Historical Marsh Loss in Chesapeake Bay, USA. Estuaries and Coasts **41**: 940–951. doi:10.1007/s12237-017-0336-9

Schuerch, M., T. Spencer, S. Temmerman, and others. 2018. Future response of global coastal wetlands to sea-level rise. Nature **561**: 231–234. doi:10.1038/s41586-018-0476-5

Smith, A. J., and E. M. Goetz. 2021. Climate change drives increased directional movement of landscape ecotones. Landsc. Ecol. doi:10.1007/s10980-021-01314-7

Smith, A. J., and M. L. Kirwan. 2021. Sea Level-Driven Marsh Migration Results in Rapid Net Loss of Carbon. Geophys. Res. Lett. **48**. doi:10.1029/2021GL092420

Smith, J. A. M. 2013. The Role of Phragmites australis in Mediating Inland Salt Marsh Migration in a Mid-Atlantic Estuary. PLoS One **8**. doi:10.1371/journal.pone.0065091

St-Laurent, P., M. A. M. Friedrichs, R. G. Najjar, E. H. Shadwick, H. Tian, and Y. Yao. 2020. Relative impacts of global changes and regional watershed changes on the inorganic carbon balance of the Chesapeake Bay. Biogeosciences **17**: 3779–3796. doi:10.5194/bg-17-3779-2020

Stevenson, J. C., M. S. Kearney, and E. C. Pendleton. 1985. Sedimentation and erosion in a Chesapeake Bay brackish marsh system. Mar. Geol. **67**: 213–235. doi:10.1016/0025-3227(85)90093-3

Sweet, W. V., R. E. Kopp, C. P. Weaver, J. Obeysekera, R. M. Horton, E. R. Thieler, and C. Zervas. 2017. Global and Regional Sea Level Rise Scenarios for the United States. NOAA Technical Report NOS CO-OPS 083.

Syvitski, J. P. M., C. J. Vorosmarty, A. J. Kettner, and P. Green. 2005. Impact of Humans on the Flux of Terrestrial Sediment to the Global Coastal Ocean. Science (80-. ). **308**: 376–380. doi:10.1126/science.1109454

Thorne, K., G. MacDonald, G. Guntenspergen, and others. 2018. U.S. Pacific coastal wetland resilience and vulnerability to sea-level rise. Sci. Adv. **4**. doi:10.1126/sciadv.aao3270

Titus, J. G., D. E. Hudgens, D. L. Trescott, and others. 2009. State and local governments plan for development of most land vulnerable to rising sea level along the US Atlantic coast. Environ. Res. Lett. **4**. doi:10.1088/1748-9326/4/4/044008

Torio, D. D., and G. L. Chmura. 2013. Assessing Coastal Squeeze of Tidal Wetlands. J. Coast. Res. **29**: 1049–1061. doi:10.2112/jcoastres-d-12-00162.1

Törnqvist, T. E., D. R. Cahoon, J. T. Morris, and J. W. Day. 2021. Coastal Wetland Resilience, Accelerated Sea-Level Rise, and the Importance of Timescale. AGU Adv. **2**. doi:10.1029/2020av000334

U.S. Fish and Wildlife Service. 2018. National Wetlands Inventory: Wetlands Mapper.

Ury, E. A., X. Yang, J. P. Wright, and E. S. Bernhardt. 2021. Rapid deforestation of a coastal landscape driven by sea-level rise and extreme events. Ecol. Appl. **31**. doi:10.1002/eap.2339

USGS. 2020. USGS Watershed Boundary Dataset (WBD) for 2-digit Hydrologic Unit - 02 (published 20201203). ScienceBase.

White, E. E., E. A. Ury, E. S. Bernhardt, and X. Yang. 2021. Climate Change Driving Widespread Loss of Coastal Forested Wetlands Throughout the North American Coastal Plain. Ecosystems. doi:10.1007/s10021-021-00686-w

White, E., and D. Kaplan. 2017. Restore or retreat? saltwater intrusion and water management in coastal wetlands. Ecosyst. Heal. Sustain. **3**. doi:10.1002/ehs2.1258

Williams, K., K. C. Ewel, R. P. Stumpf, and others. 1999. Sea-Level Rise and Coastal Forest Retreat on the West Coast of Florida , USA. Ecology **80**: 2045–2063.

Yao, Q., and K. B. Liu. 2017. Dynamics of marsh-mangrove ecotone since the mid-Holocene: A palynological study of mangrove encroachment and sea level rise in the Shark River Estuary, Florida. PLoS One **12**: 1–18. doi:10.1371/journal.pone.0173670

## Figures

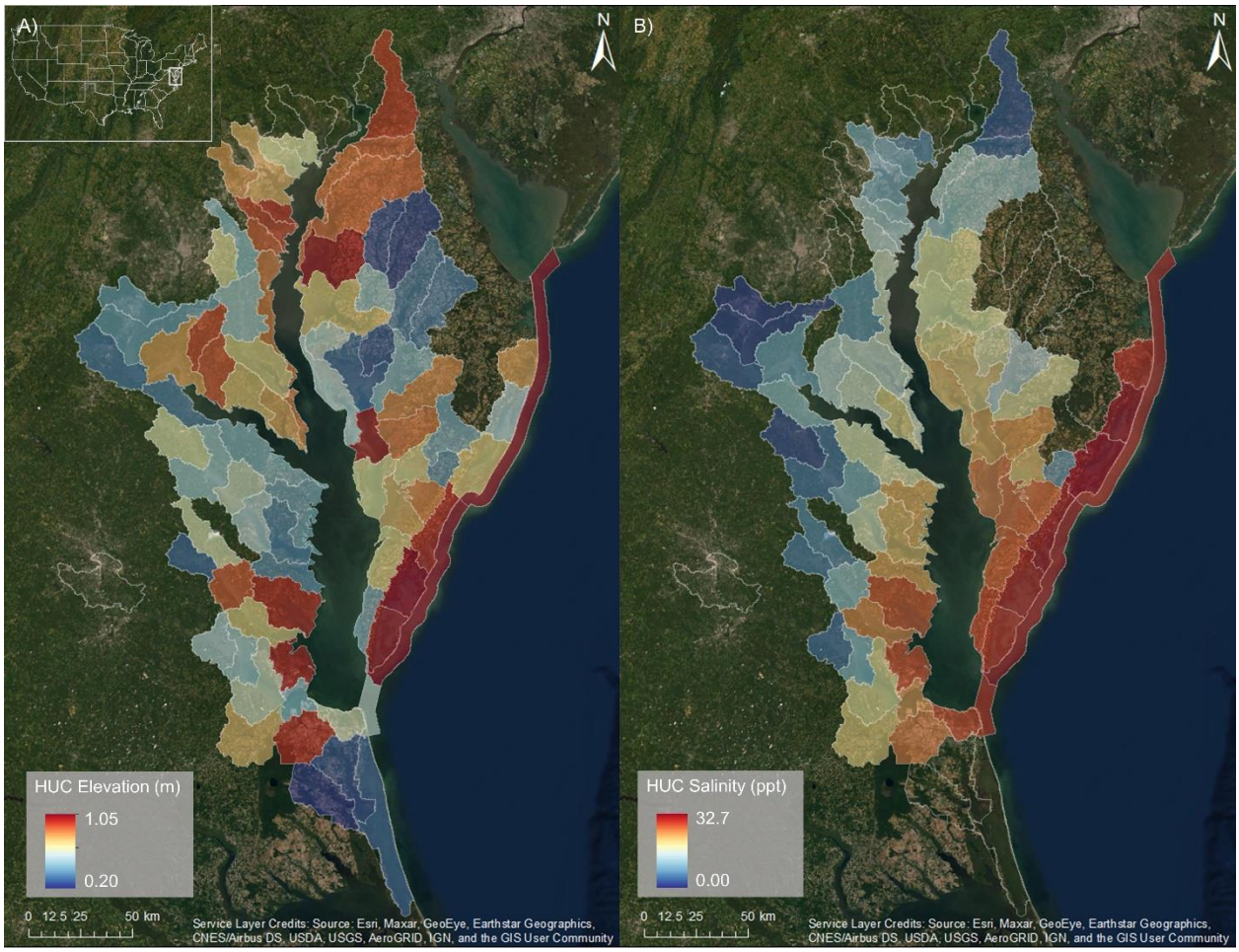


Figure 1. A) Median elevation (m NAVD88) of marsh-forest boundaries for 81 HUC10 units; 5 additional units have no color as there were discrepancies in the underlying elevation data or there were insufficient points in that unit. Median elevation was taken from all points within each HUC unit. For specific median elevation values of each HUC, see Supplemental Table 3. B) Median salinity for 68 watersheds which had sufficient salinity data based on model output provided by St-Laurent et al., 2020. Threshold elevation and salinity are positively correlated ($R^2 = 0.3$, $p = 0.03$). Salinity data were not used in our analyses other than to interpret possible sources of variability in threshold elevations. Data used to generate this figure are available in the Metadata (Molino et al., 2022).

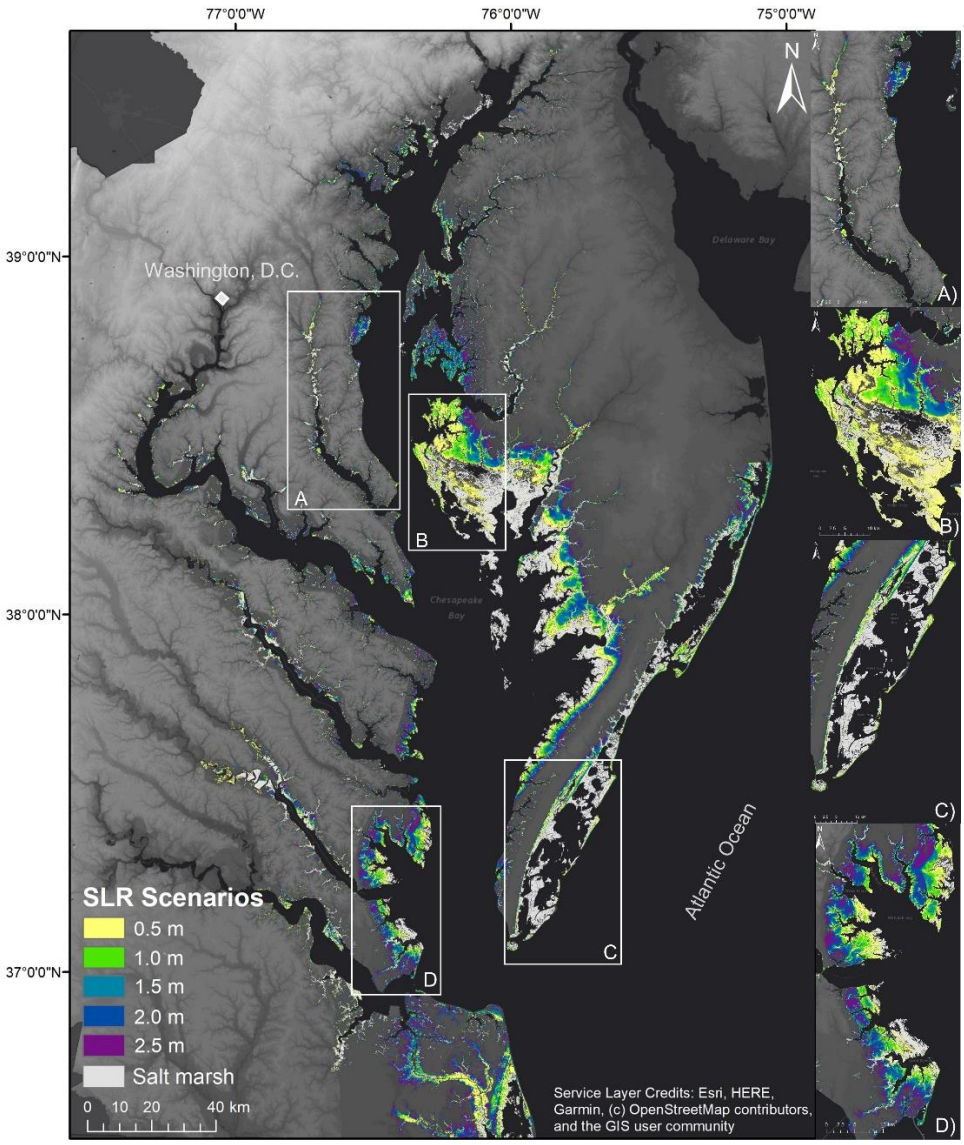


Figure 2. Potential upland converted to marsh under five generalized sea level rise scenarios. Current tidal marsh area based on the National Wetlands Inventory (NWI) emergent wetland class is depicted in light gray. A) Patuxent River, Maryland; B) Blackwater, Maryland; C) Atlantic coastal lagoons; D) Mobjack Bay, Virginia. Data used to generate this figure are available in the Metadata (Molino et al., 2022).

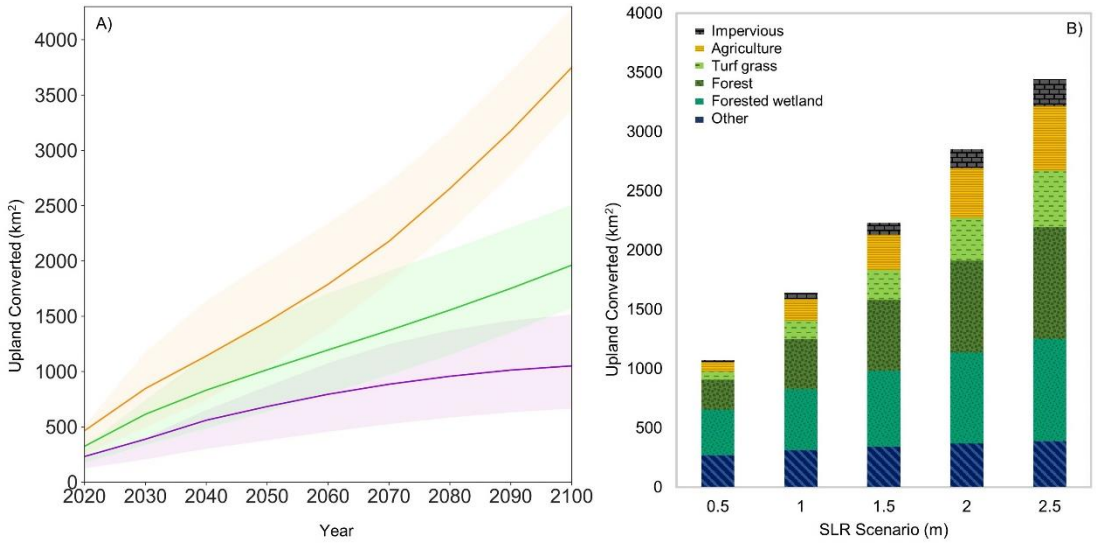


Figure 3. A) Potential upland area converted to marsh under three NOAA sea level rise scenarios. Sea level scenarios follow Sweet et al., 2017, where Low scenario (0.45 m) is in purple, Intermediate scenario (1.22 m) is in green, and High scenario (2.66 m) is in orange. Uncertainty envelopes account for root mean square error (RMSE) of the underlying elevation data (Gesch 2012). B) Land use type of potential upland converted to marsh under five generalized sea level rise scenarios. Categories based on merged classes from the Chesapeake Conservancy High-Resolution Land Use and Land Class datasets (Supp. Table 2).

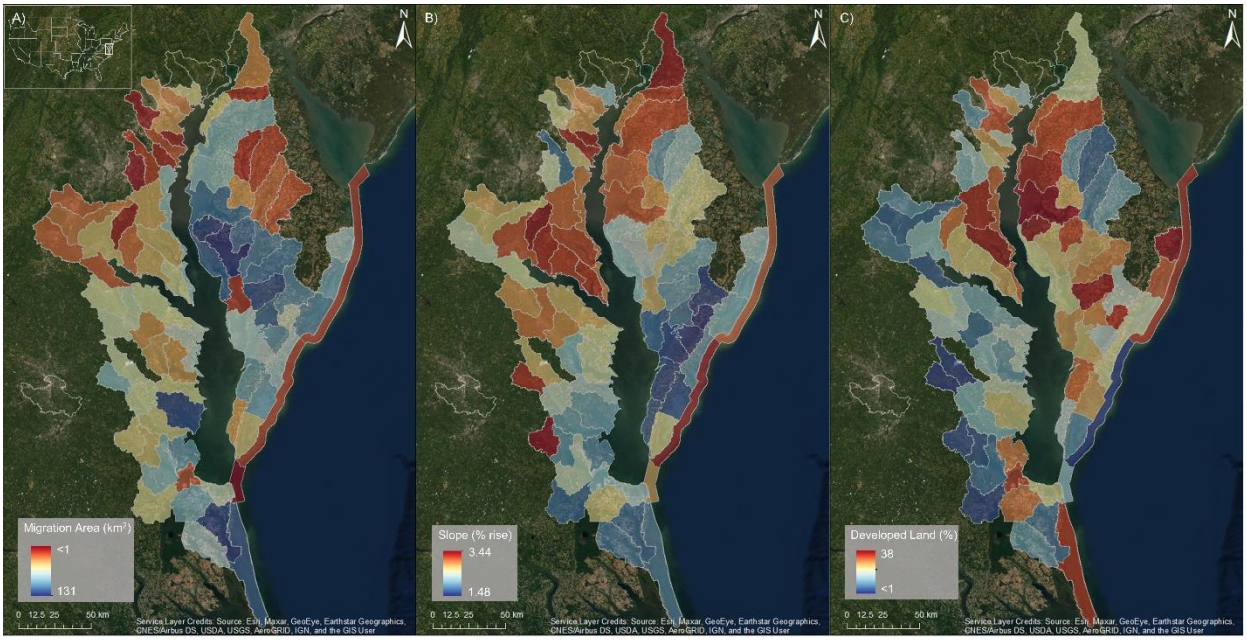


Figure 4. A) Estimates of marsh migration area under 1.0 m of sea level rise (SLR) for each HUC10 watershed; B) Median slope for each HUC10 watershed calculated from slope values at the tidal marsh-forest boundary provided by Molino et al., 2021. C) Percent developed land (impervious and agricultural) within the potential marsh migration area for 1.0 m of SLR. Land use classes based on the Chesapeake Conservancy High-Resolution Land Use and Land Cover projects (Chesapeake Conservancy 2018a; b).

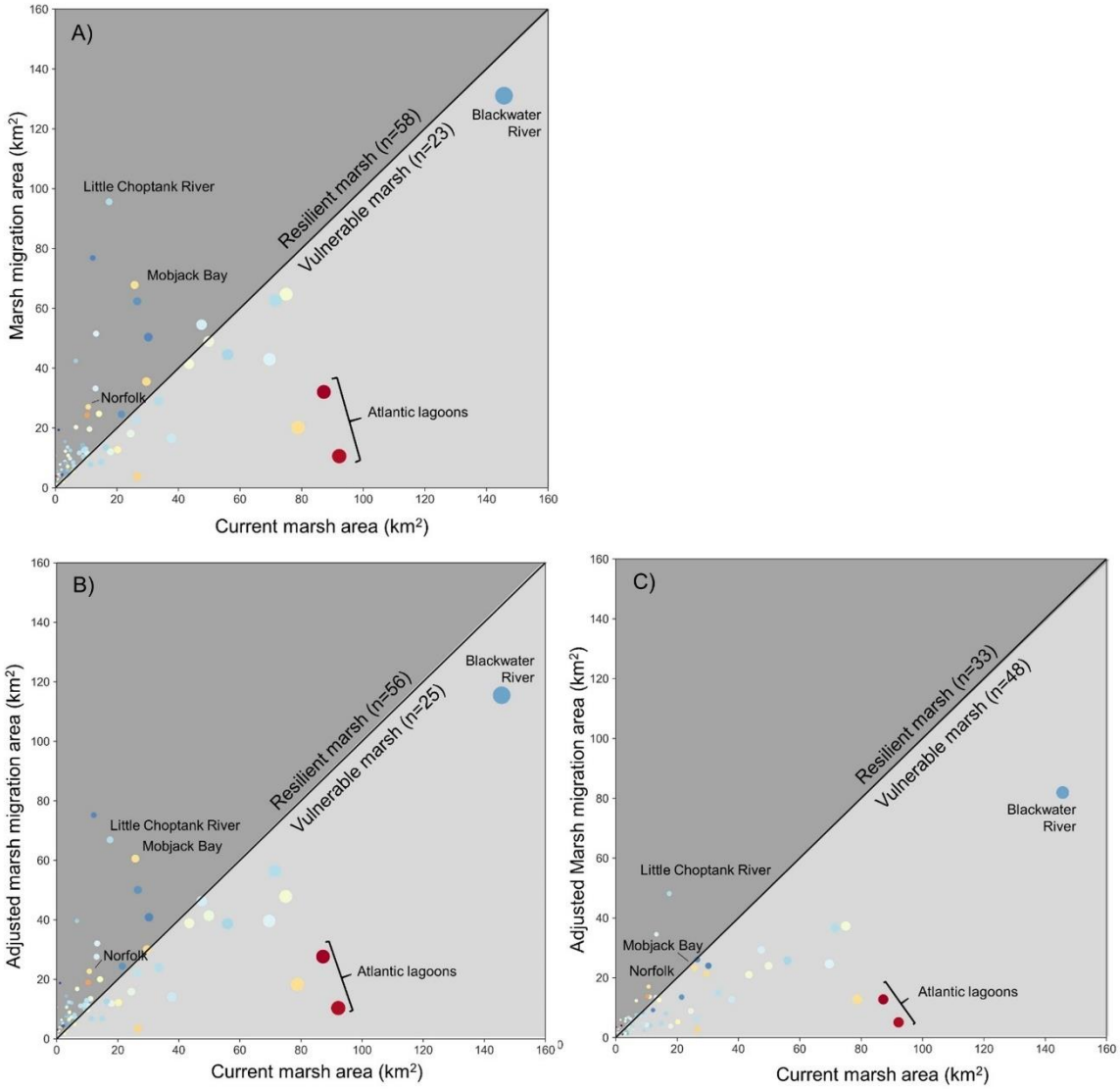


Figure 5. A) Estimates of marsh migration area under 1.0 m of sea level rise plotted against current marsh area (National Wetlands Inventory) for each HUC10 watershed; B) Estimates of marsh migration area under 1.0 m of sea level rise with developed land (agriculture and impervious) removed plotted against current marsh area for each HUC10 watershed. C) Estimates of marsh migration area under 1.0 m of sea level rise with terrestrial forest and forested wetlands removed plotted against current tidal marsh area for each HUC10 watershed. Dots are colored to represent the watershed threshold elevation value from Figure 1A where blue is low threshold elevation and red is high threshold elevation. Dot size corresponds to current marsh extent within the watershed. Data points above black line is 1:1 line represent watersheds with resilient marsh, where marsh migration could compensate for even a complete loss of existing tidal marsh. Mobjack Bay (Virginia) and Blackwater River (Maryland) are examples of high marsh migration watersheds, while the Atlantic lagoons are representative of watersheds with low marsh migration potential. Norfolk (Elizabeth River watershed in Virginia) is an example of a watershed with high impervious cover, whereas Little Choptank River (Maryland) is representative of watersheds with high agricultural land use within the marsh migration area. Data used to generate this figure are available in the Metadata (Molino et al., 2022).

## Supplemental Information

*Detailed Methods*

*Study area*

Chesapeake Bay is microtidal, with the highest mean tidal range of 0.9 m at the mouth, and the lowest mean tidal range of 0.3 m at Annapolis, Maryland (Xiong and Berger 2010). Like much of the Mid-Atlantic, Chesapeake Bay is a global hotspot of relative sea level rise due to regional subsidence coupled with weakening of the Gulf Stream (Engelhart et al. 2009; Sallenger et al. 2012). Relative rates of sea level rise in the 1930s were 1-3 mm/yr[1] . In 2011, SLR rates were 4-11 mm/yr and accelerating (Ezer and Corlett 2012; Ezer and Atkinson 2015). Low marsh vegetation typically includes *Spartina alterniflora*, and high marsh vegetation includes *Spartina patens*, *Distichlis spicata*, and *Juncus romerianus* (Perry et al. 2001). Coastal terrestrial forests which exist upland to adjacent marshes within this low elevation coastal area are typically comprised of *Pinus taeda* and *Juniperus virginiana* (Perry et al. 2001). Freshwater forested wetlands are primarily dominated by *Nyssa biflora* and *Acer rubrum* (Noe et al. 2021). Bands of *Phragmites australis* often occur at the marsh-forest boundary and are a sign of ecosystem change as the invasive reed colonizes areas of disturbance before marsh vegetation can establish (Smith 2013).

Part of the Mid-Atlantic, the Chesapeake Bay region is dominated by forest, cultivated/pastureland, and developed land uses (Epanchin-Niell et al. 2017). These land uses are distributed heterogeneously in the low-lying areas immediately surrounding Chesapeake Bay. Rural land uses, such as forests and palustrine forested wetlands, are the dominate land use classes. Southeastern Virginia, the Hampton Roads region, holds the majority of developed land use near the coast and has the highest concentration of people at risk from inundation with sea level rise in the region (Hauer et al. 2016). The Eastern Shore of Maryland and Virginia contains widespread agricultural land uses, including soybean fields and poultry production (USDA 2019).

Interestingly, the Chesapeake Bay region well represents the United States coastline which is largely rural, with pockets of major development. Along the North Atlantic Coastal Plain, 96% of land use within 1-m of sea level rise is rural (Epanchin-Niell et al. 2017), which includes our forest and forested wetland categories. Under higher sea level scenarios, 74% of U.S. watersheds vulnerable to sea level rise consist of inundated land that is predominantly rural, non-tidal wetlands, while only 16% of watersheds have developed land uses predominantly at risk for inundation (Holmquist et al. 2021). There are high concentrations of the U.S. population in major urban centers along the coast, typically not associated with the Chesapeake Bay. However, the Chesapeake Bay region (Virginia, Maryland, Washington D.C.) has the 5$^{th}$ largest population at risk from 0.9 m of sea level rise, behind only Florida, Louisiana, California, and New Jersey (Hauer et al. 2016); this is based on 2010 Census Block Groups and is projected to increase with population growth. The largely rural nature of the Chesapeake Bay with pockets of concentrated development makes this region generally representative of the U.S. coast as a whole, and well positioned for a discussion of marsh migration potential beyond the Mid-Atlantic. The United States has a much lower coastal population compared to other countries located in regions of the world where marshes are prevalent (CIESIN - Columbia University 2017). In northwestern Europe and Asia, extensive levee systems protect these coastal

[1] https://tidesandcurrents.noaa.gov/sltrends/regionalcomparison.html?region=USNA

populations, and limit the ability of marshes to migrate laterally (Kabat et al. 2005; Ma et al. 2014; Schuerch et al. 2018). This makes understanding where marshes have the potential to migrate landward in the United States increasingly important for estimates of future global marsh extent.

*Data sources*

The marsh-forest boundary points were obtained from a previously delineated marsh-forest boundary dataset comprised of over 200,000 points at a 30-m resolution along marsh-forest boundaries throughout Chesapeake Bay (Figure 1A) (Molino et al. 2020, 2021). This dataset used the National Wetlands Inventory (NWI) estuarine intertidal emergent wetlands category for salt marsh extent and forest data from the Chesapeake Conservancy to determine the boundary using geographic information system (GIS) analyses (Chesapeake Conservancy 2018a; b; U.S. Fish and Wildlife Service 2018). To determine the elevation along this boundary, we used the U.S. Geological Survey (USGS) Coastal National Elevation Database (CoNED) Topobathymetric Digital Elevation Model (Figure 1B), which has a 1-m resolution (Danielson and Tyler 2016). Current salt marsh extent within Chesapeake Bay was determined from the NWI shapefiles (U.S. Fish and Wildlife Service 2018).

We used two different SLR projections for this study. The first were general SLR estimates of 0.5, 1.0, 1.5, 2.0 and 2.5 m. The second sea level rise projections were based on the Sweet et al., 2017 projections provided at each National Oceanographic and Atmospheric Administration (NOAA) tide gauge (Sweet et al. 2017). We used the projections for tide gauges which fell within our study region and calculated a Delauney Triangulation between the points. We then took a spatially weighted average to determine a single SLR value for the entire Chesapeake Bay. This method was repeated at every 10-year time step for each NOAA sea level rise scenario we considered: global Low (0.3 m), Intermediate (1.0 m), and High (2.0 m) scenario estimates for 2100 (corresponding to 0.45, 1.22, and 2.66 m of SLR, respectively) (Sweet et al. 2017).

Land use of area converted under the general SLR scenarios was assessed using the Chesapeake Conservancy High Resolution (1 m) Land Use and Land Cover datasets (Chesapeake Conservancy 2018a; b). We merged the land use types into five categories: forest (value = 8), turf grass (values = 9, 11, 12, 13, 15), agriculture (values = 16, 17), impervious (values = 1, 2, 3), and other (values = 5, 6, 7, 10, 14) (Supplemental Table 2). A sixth category was also included, forested wetlands, which was calculated by the overlap in land use wetland classes (values = 5, 6, 7) and the land cover tree canopy class (value = 3). This category was included separately from the wetland and forest categories because the physiographic position of forested wetlands results in a higher sensitivity of this ecosystem to flooding and salinity stresses (Doyle et al. 2007). The "other" category includes mixed open and mixed impervious as well as marsh that is located at elevations above the median threshold value for each watershed. For a given threshold elevation, we assume all land below this value is already marsh, and all land above this value is not marsh. However, because the threshold is based on the median elevation of all the marsh-forest boundary points, there is land below the threshold that is not marsh (i.e. forests and forested wetlands), and there is land above the median that is already marsh. We quantified the forest and forested wetland areas below threshold elevations for each watershed and found that it was greater than the area of marsh currently above the threshold elevation. Therefore, we include marsh above the threshold elevation in our estimates of potential upland

area converted as a conservative estimate for the forest and forested wetland area below the threshold elevation which we assume will convert to marsh under each future SLR scenario.

*Analytical approach*

We quantified the area between the current marsh-forest boundary and multiple increments of sea level rise in ArcMap 10.7 to obtain an estimate of potential marsh migration area for the entire Chesapeake Bay coastal plain (Enwright et al. 2016). We took the points from the previously delineated marsh-forest boundary dataset for the Chesapeake Bay (Molino et al. 2020, 2021) and extracted the elevation of each point from the USGS CoNED topobathy (Figure 1B). We then eliminated points which were located along boundaries with >4% slope to minimize error associated with offset in lateral position. Additionally, points with an elevation value of less than 0.1 m NAVD88 (North American Vertical Datum of 1988) were removed as these were often located in marsh channels or other bodies of water, and points with an elevation greater than 2.0 m NAVD88 were removed as these were mostly located in residential areas adjacent to marshes. Together, these steps helped minimize any potential error associated with gross misclassification of the marsh-forest boundary. The inaccuracy of the point locations was due to misrepresentation of the marsh-forest boundary delineated prior to this study.

We then calculated the median elevation of the marsh-forest boundary, hereafter referred to as the threshold elevation, for USGS HUC10 (Hydrologic Unit) watersheds (USGS 2020). This approach allows us to account for spatial variability in the processes that likely influence the threshold elevation (e.g. tidal range, salinity) and quantify marsh migration at the watershed scale. The points along the marsh-forest boundary were contained within 86 HUC10 watersheds along the Chesapeake Bay (Figure 1C) (Molino et al. 2022). Four watersheds were removed because they contained areas of abrupt elevation shifts (>1 m change) corresponding to where individual elevation datasets had been combined to create the CoNED topobathy. For 11 watersheds that contained less than 100 points each, the threshold elevation was determined by additionally including all points from a neighboring watershed with similar topobathymetric features. One watershed that contained less than ten points was removed as it had no neighboring watersheds from which to combine points. Thus, our analysis includes 81 of 86 HUC10 watersheds surrounding Chesapeake Bay where elevation of the marsh-forest boundary can be most precisely defined.

To determine areas of future marsh migration, we added increments of sea level rise to the threshold elevation of each watershed and quantified the area between the original marsh-forest boundary and new marsh-upland boundary. To do this, we split the CoNED topobathy raster into 81 watersheds and set the unique threshold elevation for each watershed as the baseline. Below this threshold, all land was assumed to be either water or marsh. We then reclassified the raster values by adding the increment of sea level rise we were interested in to the baseline and quantifying the area in between the threshold elevation and the threshold elevation plus the SLR scenario. For example, a watershed with a threshold elevation of 0.32 m assumes that the land which would convert to marsh with 0.5 m of SLR would be land from 0.32 m to 0.82 m (0.32m + 0.50m) in elevation. We used the reclassify tool in ArcMap which quantified the raster cells whose elevation fell between these elevations for each SLR scenario. This was completed for each watershed for the general SLR scenarios as well as the Chesapeake Bay specific predictions derived from the NOAA data. Marsh migration areas for each watershed were combined for a bay-wide projection of potential marsh migration area (Molino et al. 2022). Like previous work, we only consider land available for marsh migration, and do not account for

accretion or edge erosion (Enwright et al. 2016; Borchert et al. 2018; Holmquist et al. 2021). However, we are also not accounting for processes such as peat collapse which could accelerate marsh migration (Miller et al. 2021). Following Gesch (2012), we calculated uncertainty envelopes for area converted under the localized NOAA predictions by adding and subtracting the root mean square error (RMSE) of the CoNED dataset (20 cm) from the new marsh-upland elevation within each watershed (Danielson and Tyler, 2016).

Land use inundated under each SLR scenario was quantified by individual watershed. To do this, we extracted the land use within the area that was projected to convert to marsh under the different sea level rise scenarios determined during the reclassification process described above. We combined these numbers for a bay-wide assessment of land use within the potential marsh migration area. This allowed us to examine how local variations in land use influenced marsh migration area regionally.

*Limitations*

We assume that the threshold elevations determined from the marsh-forest boundary are representative of marsh-upland boundaries in general given that forested uplands make up more than half of the upland land use and that other upland land use types, such as agricultural land, are often separated from wetlands by a thin band of forest. Preliminary results from analyses of marsh-agriculture, forested wetlands, impervious, and turf boundaries suggest threshold elevations for other land uses are similar to that of the marsh-forest boundary (Supplemental Table 1). The marsh-agricultural boundary was significantly higher in elevation from the marsh-forest boundary, which we hypothesize is for two reasons. First, some agricultural areas are located on high elevation river bluffs. The very steep, but narrow change in elevation means that the boundary between these two land uses is at a very high elevation. The second and most common reason is that agricultural areas often have small earthen levees (~1 m in height) to protect them from tidal inundation. Without these anthropogenic features, the natural elevation between marsh-agriculture would likely be similar to the other boundary elevations. However, more work is needed to refine this method for other land uses.

It should be noted that we do not directly assess the effect of connectivity on our calculated marsh migration area. When using high resolution digital elevation models for inundation estimates, it is possible that some isolated low-lying areas will be counted in the area of potential marsh migration even though they are not hydrologically connected to other marsh or water. However, this issue is minimized because our approach to calculating potential marsh migration includes only land that is above a watershed's threshold elevation. For example, there is a quarry in a northern watershed of Chesapeake Bay that is excluded from the analysis because it has elevations below the watershed's threshold elevation. As described earlier, our approach explicitly calculates marsh migration by counting the number of raster cells with elevations between the threshold elevation and the threshold elevation plus an increment of sea level rise (i.e., migration area includes locations with elevations between 0.61 and 1.61 m for a watershed with a threshold elevation of 0.61 m and a 1 m increment of sea level rise). In that example, elevations between 0.61-1.61 m NAVD would be counted as potential migration area, regardless of connectivity. However, previous inundation mapping with high resolution (6 m) DEMs in coastal North Carolina suggests that connectivity effects are minimal for SLR scenarios greater than about 0.4 m (Poulter and Halpin 2008). For a 1 m SLR scenario, there was less than 3% difference in cumulative area inundated between approaches that did not consider connectivity and those which considered 4-sided or 8-sided connectivity (Poulter and Halpin 2008). Six of our

eight sea level rise scenarios use projections greater than 1 m which suggests that the overestimation of area from low-lying area upslope is minimal. Nevertheless, future steps quantifying this potential area would improve local estimates of marsh migration on a watershed scale.

Additionally, our quantification of land use is limited by the accuracy of the land use and land cover datasets. In particular, forest and forested wetlands can be confused by remote sensing techniques (McCarthy et al. 2018). As a result, we combine all forested areas when delineating the marsh-forest boundary as those measurements rely on precise delineation between ecosystem types. Future work could benefit from improvements in identifying between forest and forested wetlands.

## References


Borchert, S. M., M. J. Osland, N. M. Enwright, and K. T. Griffith. 2018. Coastal wetland adaptation to sea level rise: Quantifying potential for landward migration and coastal squeeze. J. Appl. Ecol. **55**: 2876–2887. doi:10.1111/1365-2664.13169

Chesapeake Conservancy. 2018a. Land Use Data Project 2013/2014.

Chesapeake Conservancy. 2018b. Land Cover Data Project 2013/2014.

CIESIN - Columbia University. 2017. Gridded Population of the World, Version 4 (GPWv4): Population Count Adjusted to Match 2015 Revision of UN WPP Country Totals, Revision 10.

Danielson, J., and D. Tyler. 2016. Topobathymetric Model for Chesapeake Bay Region - District of Columbia, States of Delaware, Maryland, Pennsylvania, and Virginia, 1859 to 2015.

Doyle, T. W., C. P. O'Neil, M. P. V. Melder, A. S. From, and M. M. Palta. 2007. Tidal freshwater swamps of the Southeastern United States: Effects of land use, hurricanes, sea-level rise, and climate change, p. 1–28. *In* W.H. Conner, T.W. Doyle, and K.W. Krauss [eds.], Ecology of Tidal Freshwater Forested Wetlands of the Southeastern United States. Springer.

Engelhart, S. E., B. P. Horton, B. C. Douglas, W. R. Peltier, and T. E. Törnqvist. 2009. Spatial variability of late Holocene and 20th century sea-level rise along the Atlantic coast of the United States. Geology **37**: 1115–1118. doi:10.1130/G30360A.1

Enwright, N. M., K. T. Griffith, and M. J. Osland. 2016. Barriers to and opportunities for landward migration of coastal wetlands with sea-level rise. Front. Ecol. Environ. **14**: 307–316. doi:10.1002/fee.1282

Epanchin-Niell, R., C. Kousky, A. Thompson, and M. Walls. 2017. Threatened protection: Sea level rise and coastal protected lands of the eastern United States. Ocean Coast. Manag. **137**: 118–130. doi:10.1016/j.ocecoaman.2016.12.014

Ezer, T., and L. P. Atkinson. 2015. Sea Level Rise in Virginia – Causes, Effects and Response. Va. J. Sci. **66**. doi:10.25778/8w61-qe76

Ezer, T., and W. B. Corlett. 2012. Is sea level rise accelerating in the Chesapeake Bay? A demonstration of a novel new approach for analyzing sea level data. Geophys. Res. Lett. **39**: 1–6. doi:10.1029/2012GL053435

Gesch, D. B. 2012. Elevation Uncertainty in Coastal Inundation Hazard Assessments, p. 121–140. *In* S. Cheval [ed.], Natural Disasters. InTech.

Hauer, M. E., J. M. Evans, and D. R. Mishra. 2016. Millions projected to be at risk from sea-level rise in the continental United States. Nat. Clim. Chang. **6**: 691–695. doi:10.1038/nclimate2961

Holmquist, J. R., L. N. Brown, and G. M. MacDonald. 2021. Localized Scenarios and Latitudinal Patterns of Vertical and Lateral Resilience of Tidal Marshes to Sea-Level Rise in the Contiguous United States. Earth's Futur. **9**. doi:10.1029/2020ef001804

Kabat, P., W. van Vierssen, J. Veraart, P. Vellinga, and J. Aerts. 2005. Climate proofing the Netherlands. Nature **438**: 283–284. doi:10.1038/438283a

Ma, Z., D. S. Melville, J. Liu, and others. 2014. Rethinking China's new great wall. Science (80-. ). **346**: 912–914. doi:10.1126/science.1257258

McCarthy, M. J., K. R. Radabaugh, R. P. Moyer, and F. E. Muller-Karger. 2018. Enabling efficient, large-scale high-spatial resolution wetland mapping using satellites. Remote Sens. Environ. **208**: 189–201. doi:10.1016/j.rse.2018.02.021

Miller, C. B., A. B. Rodriguez, and M. C. Bost. 2021. Sea-level rise , localized subsidence , and increased storminess promote saltmarsh transgression across low-gradient upland areas. Quat. Sci. Rev. **265**. doi:10.1016/j.quascirev.2021.107000

Molino, G. D., J. A. Carr, N. K. Ganju, and M. L. Kirwan. 2022. Spatial Variability in Marsh Vulnerability and Coastal Forest Loss in Chesapeake Bay ver 1.doi:https://doi.org/10.6073/pasta/5f67dfab12021a36aa1886604844fbaa

Molino, G. D., Z. Defne, A. L. Aretxabaleta, N. K. Ganju, and J. A. Carr. 2021. Quantifying Slopes as a Driver of Forest to Marsh Conversion Using Geospatial Techniques: Application to Chesapeake Bay Coastal-Plain, United States. Front. Environ. Sci. **9**. doi:10.3389/fenvs.2021.616319

Molino, G. D., Z. Defne, N. K. Ganju, J. A. Carr, G. R. Gutenspergen, and D. C. Walters. 2020. Slope Values Across Marsh-Forest Boundary in Chesapeake Bay Region, USA.doi:10.5066/P9EJ6PGT

Noe, G. B., N. A. Bourg, K. W. Krauss, J. A. Duberstein, and C. R. Hupp. 2021. Watershed and estuarine controls both influence plant community and tree growth changes in tidal freshwater forested wetlands along two U.S. Mid-Atlantic rivers. Forests **12**. doi:10.3390/f12091182

Perry, J. E., T. A. Barnard, J. G. Bradshaw, and others. 2001. Creating Tidal Salt Marshes in the Chesapeake Bay. J. Coast. Res. 170–191.

Poulter, B., and P. N. Halpin. 2008. Raster modelling of coastal flooding from sea-level rise. Int. J. Geogr. Inf. Sci. **22**: 167–182. doi:10.1080/13658810701371858

Sallenger, A. H., K. S. Doran, and P. A. Howd. 2012. Hotspot of accelerated sea-level rise on the Atlantic coast of North America. Nat. Clim. Chang. **2**: 884–888. doi:10.1038/nclimate1597

Schuerch, M., T. Spencer, S. Temmerman, and others. 2018. Future response of global coastal wetlands to sea-level rise. Nature **561**: 231–234. doi:10.1038/s41586-018-0476-5

Smith, J. A. M. 2013. The Role of Phragmites australis in Mediating Inland Salt Marsh Migration in a Mid-Atlantic Estuary. PLoS One **8**. doi:10.1371/journal.pone.0065091

Sweet, W. V., R. E. Kopp, C. P. Weaver, J. Obeysekera, R. M. Horton, E. R. Thieler, and C. Zervas. 2017. Global and Regional Sea Level Rise Scenarios for the United States. NOAA Technical Report NOS CO-OP 83.

U.S. Fish and Wildlife Service. 2018. National Wetlands Inventory: Wetlands Mapper.

USDA. 2019. 2017 Census Volume 1, Chapter 2: County Level. Census Agric.

USGS. 2020. USGS Watershed Boundary Dataset (WBD) for 2-digit Hydrologic Unit - 02 (published 20201203). ScienceBase.

Xiong, Y., and C. R. Berger. 2010. Chesapeake Bay Tidal Characteristics. J. Water Resour. Prot. **2**: 619–628. doi:10.4236/jwarp.2010.27071

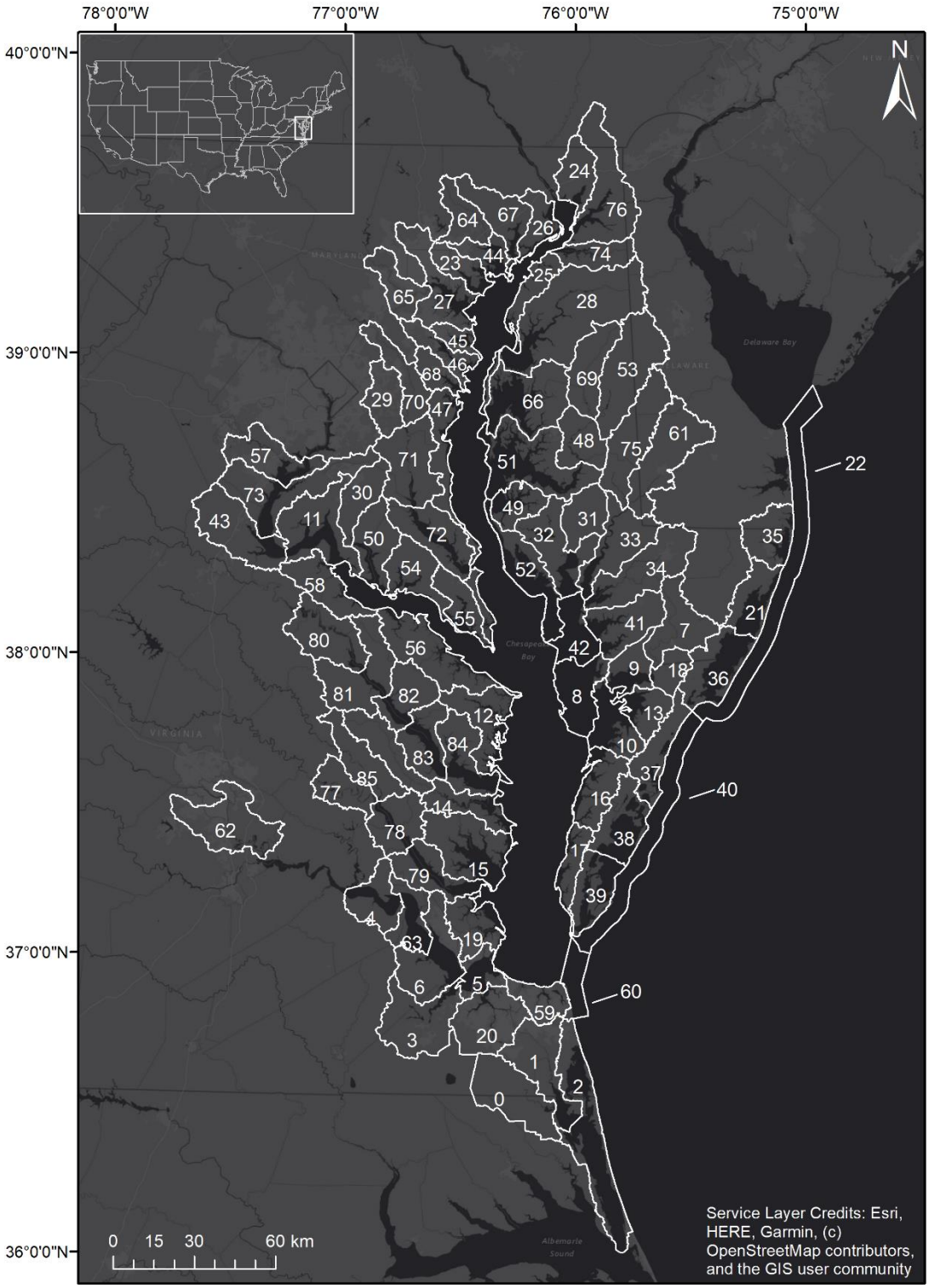
78°0'0"W
77°0'0"W
76°0'0"W
75°0'0"W
40°0'0"N
39°0'0"N
38°0'0"N
37°0'0"N
36°0'0"N
N
0 15 30 60 km
Service Layer Credits: Esri, HERE, Garmin, (c) OpenStreetMap contributors, and the GIS user community

Supp. Figure 1: Original 86 HUC10 (Hydrologic Unit) watersheds for the Chesapeake Bay region considered for this study, labeled with the corresponding ID number. Watersheds 24, 26, 62, 64, and 67 were not used in the analyses due to lack of a reliable number of points or issues with the underlying elevation data. A shapefile of these HUC watersheds is available in the Metadata (Molino et al., 2022). Inset shows location of study area on the Mid-Atlantic coast of

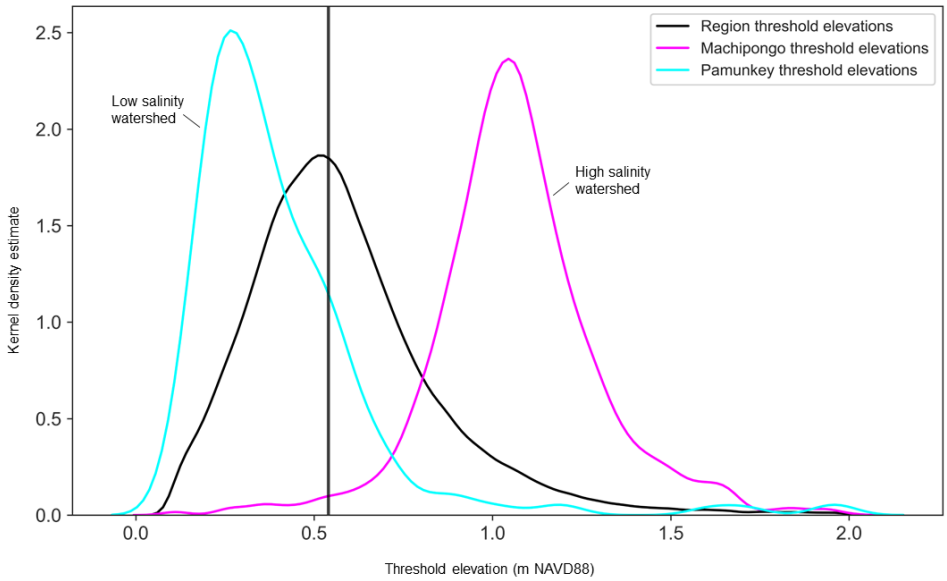


Supp. Figure 2: Kernel density estimates of threshold elevation for all points in Chesapeake Bay region (black) with median (0.54 m) plotted as black line. Threshold elevation points within Pamunkey (teal) and Machipongo (pink) watersheds, which have comparable tidal range (0.9-1.15 m from NOAA VDATUM (https://vdatum.noaa.gov/; date accessed December 12, 2020)) but are end members of salinity (1.4 and 32.0 ppt respectively) highlighting the influence of salinity on threshold elevation (St-Laurent et al., 2021). The Pamunkey watershed is HUC ID# 77 (Supp. Figure 1), containing the Pamunkey River which is a tributary of the York River and ultimately the Chesapeake Bay. The Machipongo watershed is HUC ID# 38 (Supp. Figure 1) which contains a portion of the Atlantic coastal lagoons. Data used to generate this figure are available in the Metadata (Molino et al., 2022).

Supp. Table 1: Median threshold elevations for different marsh-upland boundaries in the state of Virginia, United States. The "Forest" category includes all the marsh-forest boundary points in Virginia used to determine threshold elevations in this study. "Forested wetlands" are a subset of the "Forest" points. For a description of each category, see Supp. Table 2.

| **Marsh-upland boundaries - Virginia** | **Median threshold elevation (m NAVD88)** |
|---|---|
| Forest | 0.56 |
| Forested wetlands | 0.59 |
| Agricultural | 1.06 |

| | |
|---|---|
| Impervious | 0.55 |
| Turf grass | 0.63 |

Supp. Table 2: Chesapeake Conservancy High Resolution (1 m) Land Use categories included in the merged categories used in this study. Specific code from raster file included in parentheses. Forested wetlands were created using the overlap in Chesapeake Conservancy Land Use wetlands category and the Chesapeake Conservancy Land Cover Forest category

| **Merged Land Use Category** | **Chesapeake Conservancy Land Use Category** |
|---|---|
| Impervious | Impervious, roads (1), impervious, non-roads (2), tree canopy over impervious (3) |
| Agriculture | cropland (16), pastureland (17) |
| Turf grass | Tree canopy over turf (9), fractional turf, small (11), fractional turf, medium (12), fractional turf, large (13), turf grass (15) |
| Forest | Forest (8) |
| Forested wetlands | Tidal wetland (5), floodplain wetland (6), other wetland (7) overlap with CC Land Cover tree canopy (3) |
| Other | Tidal wetland (5), floodplain wetland (6), other wetland (7), mixed open (10), fractional impervious (14) |

Supp. Table 3: HUC10 watersheds considered for this study labeled with the corresponding ID number, threshold elevation, and total marsh migration area. Watersheds not considered in the analyses (24, 26, 62, 64, and 67) have values of NA. Please note that watersheds 19 and 23 have the same name – this is not a mistake, those are the names from the original source data. Instead we differentiate them by their unique HUC ID numbers. For the location of each watershed, see Supp. Figure 1.

| **HUC ID#** | **Name** | **Elevation (m NAVD88)** | **Marsh Migration Area 1.0m SLR ($km^2$)** | **Marsh Migration Area 2.5m SLR ($km^2$)** |
|---|---|---|---|---|
| 0 | Northwest River | 0.20 | 19.3 | 66.8 |
| 1 | North Landing River | 0.32 | 76.9 | 162.8 |
| 2 | Currituck Sound | 0.34 | 62.3 | 108.3 |
| 3 | Nansemond River | 0.57 | 12.0 | 17.7 |
| 4 | Powhatan Creek-James River | 0.47 | 10.7 | 18.5 |
| 5 | Pagan River-James River | 0.49 | 22.7 | 35.9 |
| 6 | Hampton Roads | 0.46 | 4.7 | 30.8 |
| 7 | Dividing Creek-Pocomoke River | 0.45 | 42.4 | 80.7 |
| 8 | Lower Tangier Sound | 0.52 | 16.5 | 17.1 |
| 9 | Marumsco Creek-Pocomoke Sound | 0.53 | 54.5 | 94.6 |

| | | | | |
|---|---|---|---|---|
| 10 | Deep Creek-Pocomoke Sound | 0.57 | 18.1 | 39.0 |
| 11 | Nanjemoy Creek-Potomac River | 0.58 | 10.4 | 26.2 |
| 12 | Great Wicomico River-Frontal Chesapeake Bay | 0.43 | 15.4 | 52.6 |
| 13 | Messongo Creek-Frontal Pocomoke Sound | 0.59 | 41.4 | 64.3 |
| 14 | Piankatank River-Frontal Chesapeake Bay | 0.41 | 12.1 | 34.9 |
| 15 | Mobjack Bay-Frontal Chesapeke Bay | 0.71 | 67.8 | 164.7 |
| 16 | Pungoteague Creek-Frontal Chesapeake Bay | 0.53 | 33.2 | 76.9 |
| 17 | Cherrystone Inlet-Frontal Chesapeake Bay | 0.43 | 8.3 | 29.5 |
| 18 | Pitts Creek-Pocomoke River | 0.42 | 14.2 | 45.6 |
| 19 | Back River-Frontal Chesapeake Bay | 0.72 | 35.5 | 98.3 |
| 20 | Elizabeth River | 0.70 | 27.1 | 143.2 |
| 21 | Upper Chincoteague Bay | 0.47 | 29.1 | 74.7 |
| 22 | Assateague Island-Atlantic Ocean | 1.05 | 3.9 | 7.5 |
| 23 | Back River-Frontal Chesapeake Bay | 0.50 | 6.1 | 15.8 |
| 24 | North East River-Frontal Chesapeake Bay | NA | NA | NA |
| 25 | Fairlee Creek-Frontal Chesapeake Bay | 0.62 | 10.8 | 24.3 |
| 26 | Romney Creek-Frontal Chesapeake Bay | NA | NA | NA |
| 27 | Patapsco River-Frontal Chesapeake Bay | 0.57 | 7.8 | 28.7 |
| 28 | Chester River | 0.63 | 24.7 | 58.5 |
| 29 | Western Branch Patuxent River | 0.51 | 1.3 | 2.2 |
| 30 | Zekiah Swamp Run | 0.65 | 2.0 | 3.9 |
| 31 | Transquaking River | 0.32 | 50.3 | 106.0 |
| 32 | Blackwater River | 0.36 | 131.0 | 181.8 |
| 33 | Lower Nanticoke River | 0.46 | 44.5 | 94.7 |
| 34 | Wicomico River | 0.58 | 48.9 | 89.6 |
| 35 | Assawoman Bay | 0.58 | 19.6 | 48.5 |
| 36 | Lower Chincoteague Bay | 0.54 | 42.9 | 61.4 |
| 37 | Metompkin Bay-Burtons Bay | 0.71 | 20.1 | 47.0 |
| 38 | Machipongo River-Hog Island Bay | 1.05 | 32.0 | 52.7 |
| 39 | Magothy Bay-Cobb Bay | 1.03 | 10.6 | 15.6 |
| 40 | Parramore Island-Atlantic Ocean | 1.05 | 4.1 | 4.5 |
| 41 | Manokin River-Frontal Tangier Sound | 0.60 | 64.7 | 112.6 |
| 42 | Upper Tangier Sound | 0.73 | 3.8 | 5.1 |
| 43 | Potomac Creek-Potomac River | 0.37 | 5.6 | 9.5 |
| 44 | Gunpowder River-Frontal Chesapeake Bay | 0.50 | 11.7 | 20.4 |
| 45 | Magothy River-Frontal Chesapeake Bay | 0.68 | 2.5 | 5.5 |

| | | | | |
|---|---|---|---|---|
| 46 | Severn River-Frontal Chesapeake Bay | 0.65 | 4.6 | 10.7 |
| 47 | Herring Bay-Frontal Chesapeake Bay | 0.60 | 20.3 | 62.3 |
| 48 | Huntington Creek-Choptank River | 0.46 | 7.8 | 16.7 |
| 49 | Little Choptank River | 0.48 | 95.6 | 122.3 |
| 50 | Wicomico River-Frontal Potomac River | 0.65 | 5.7 | 16.4 |
| 51 | Choptank River-Frontal Chesapeake Bay | 0.55 | 51.5 | 161.0 |
| 52 | Honga River-Frontal Chesapeake Bay | 0.48 | 62.6 | 63.4 |
| 53 | Watts Creek-Choptank River | 0.27 | 4.5 | 7.8 |
| 54 | Saint Clements Bay-Frontal Potomac River | 0.56 | 8.8 | 23.0 |
| 55 | Saint Marys River-Frontal Potomac River | 0.57 | 12.2 | 27.2 |
| 56 | Nomini Creek-Frontal Potomac River | 0.45 | 12.5 | 37.5 |
| 57 | Occoquan River-Potomac River | 0.42 | 5.6 | 8.7 |
| 58 | Upper Machodoc Creek-Frontal Potomac River | 0.39 | 5.1 | 10.6 |
| 59 | Lynnhaven River-Frontal Chesapeake Bay | 0.49 | 13.6 | 58.5 |
| 60 | Rudee Inlet-Atlantic Ocean | 0.48 | 0.6 | 5.0 |
| 61 | Upper Nanticoke River | 0.39 | 4.5 | 9.4 |
| 62 | Falling Creek-James River | NA | NA | NA |
| 63 | Lawnes Creek-James River | 0.47 | 10.4 | 17.9 |
| 64 | Lower Gunpowder Falls | NA | NA | NA |
| 65 | Patapsco River | 0.58 | 1.4 | 3.0 |
| 66 | Eastern Bay | 0.81 | 24.3 | 87.4 |
| 67 | Winters Run-Bush River | NA | NA | NA |
| 68 | South River-Chesapeake Bay | 0.64 | 2.9 | 6.8 |
| 69 | Tuckahoe Creek | 0.28 | 2.6 | 4.9 |
| 70 | Upper Patuxent River | 0.46 | 3.9 | 6.2 |
| 71 | Middle Patuxent River | 0.47 | 8.7 | 14.8 |
| 72 | Lower Patuxent River | 0.54 | 9.8 | 22.1 |
| 73 | Quantico Creek-Potomac River | 0.42 | 6.0 | 11.6 |
| 74 | Sassafras River | 0.63 | 3.2 | 7.3 |
| 75 | Marshyhope Creek | 0.39 | 5.9 | 12.1 |
| 76 | Elk River | 0.65 | 7.1 | 16.3 |
| 77 | Lower Pamunkey River | 0.34 | 24.6 | 31.6 |
| 78 | Upper York River | 0.65 | 12.7 | 30.1 |
| 79 | Lower York River | 0.54 | 11.7 | 28.5 |
| 80 | Occupacia Creek-Rappahannock River | 0.50 | 12.5 | 26.7 |
| 81 | Cat Point Creek-Rappahannock River | 0.46 | 13.5 | 24.4 |
| 82 | Totuskey Creek-Rappahannock River | 0.49 | 7.3 | 15.7 |

| | | | | |
|---|---|---|---|---|
| 83 | Lancaster Creek-Rappahannock River | 0.47 | 8.5 | 20.2 |
| 84 | Corrotoman River-Rappahannock River | 0.40 | 8.3 | 15.9 |
| 85 | Garnetts Creek-Mattaponi River | 0.49 | 13.0 | 21.4 |

979

Supp. Table 4: Area of uplands converted by 2100 under NOAA Low, Intermediate, and High SLR predictions and five generalized sea level rise (SLR) scenarios. Uncertainty envelopes were calculated for the NOAA scenarios based on the CoNED topobathy root mean square error (20 cm). Blank cells indicate SLR scenarios for which uncertainty estimates were not conducted.

| **NOAA SLR** | **Lower Uncertainty ($km^2$)** | **Land converted ($km^2$)** | **Upper Uncertainty ($km^2$)** |
|---|---|---|---|
| Low (0.45 m) | 664 | 1050 | 1516 |
| Intermediate (1.22 m) | 1577 | 1961 | 2504 |
| High (2.66 m) | 3374 | 3748 | 4275 |
| **General SLR (m)** | | | |
| 0.5 | | 1073 | |
| 1.0 | | 1638 | |
| 1.5 | | 2231 | |
| 2.0 | | 2852 | |
| 2.5 | | 3444 | |

980

981

982

983

Supp. Table 5: Area of land use types ($km^2$) predicted to convert to marsh under each sea level rise (SLR) scenario.

| **SLR (m)** | **Forest** | **Forested Wetlands** | **Turf Grass** | **Agriculture** | **Impervious** | **Other** | **Total ($km^2$)** |
|---|---|---|---|---|---|---|---|
| 0.5 | 252 | 383 | 69 | 79 | 20 | 271 | 1073 |
| 1 | 425 | 514 | 154 | 179 | 53 | 312 | 1638 |
| 1.5 | 599 | 639 | 253 | 301 | 98 | 341 | 2231 |
| 2 | 776 | 767 | 361 | 422 | 159 | 368 | 2852 |
| 2.5 | 945 | 863 | 475 | 545 | 227 | 389 | 3444 |

984

985

986

987

988

989

Supp. Table 6: Percentage of agricultural, impervious, and developed (combined agriculture and impervious) land use within predicted marsh migration area for 1.0 m of sea level rise (SLR) for each HUC watershed. Adjusted 1:1 has the developed land use removed from the marsh migration area when calculating the resilience index. Please note that watersheds 19 and 23 have the same name – this is not a mistake, those are the names from the original source data. Instead we differentiate them by their unique HUC ID numbers. For the location of each watershed, see Supp. Figure 1.

990

| HUC ID# | Name | Agricultural Land Use | Impervious Land Use | Total Developed Land Use | Original 1:1 | Adjusted 1:1 |
|---|---|---|---|---|---|---|
| 0 | Northwest River | 2.8% | 0.3% | 3.1% | 17.9 | 17.3 |
| 1 | North Landing River | 1.4% | 0.7% | 2.1% | 6.3 | 6.2 |
| 2 | Currituck Sound | 17.1% | 2.6% | 19.7% | 2.3 | 1.9 |
| 3 | Nansemond River | 0.0% | 0.8% | 0.9% | 0.7 | 0.7 |
| 4 | Powhatan Creek-James River | 0.3% | 0.8% | 1.0% | 70.3 | 69.6 |
| 5 | Pagan River-James River | 0.0% | 1.7% | 1.8% | 0.9 | 0.8 |
| 6 | Hampton Roads | 0.0% | 19.3% | 19.3% | 3.1 | 2.5 |
| 7 | Dividing Creek-Pocomoke River | 5.9% | 0.8% | 6.7% | 6.4 | 6.0 |
| 8 | Lower Tangier Sound | 4.4% | 10.4% | 14.9% | 0.4 | 0.4 |
| 9 | Marumsco Creek-Pocomoke Sound | 12.7% | 2.4% | 15.1% | 1.1 | 1.0 |
| 10 | Deep Creek-Pocomoke Sound | 10.0% | 2.5% | 12.5% | 0.7 | 0.6 |
| 11 | Nanjemoy Creek-Potomac River | 3.4% | 1.3% | 4.7% | 1.0 | 1.0 |
| 12 | Great Wicomico River-Frontal Chesapeake Bay | 4.9% | 2.3% | 7.2% | 4.9 | 4.6 |
| 13 | Messongo Creek-Frontal Pocomoke Sound | 4.6% | 1.5% | 6.1% | 1.0 | 0.9 |
| 14 | Piankatank River-Frontal Chesapeake Bay | 4.4% | 3.0% | 7.4% | 3.6 | 3.4 |
| 15 | Mobjack Bay-Frontal Chesapeke Bay | 8.0% | 2.6% | 10.6% | 2.6 | 2.4 |
| 16 | Pungoteague Creek-Frontal Chesapeake Bay | 15.1% | 1.8% | 16.9% | 2.5 | 2.1 |
| 17 | Cherrystone Inlet-Frontal Chesapeake Bay | 4.5% | 1.6% | 6.1% | 2.4 | 2.2 |
| 18 | Pitts Creek-Pocomoke River | 19.8% | 1.2% | 21.0% | 1.6 | 1.3 |
| 19 | Back River-Frontal Chesapeake Bay | 1.3% | 14.1% | 15.5% | 1.2 | 1.0 |
| 20 | Elizabeth River | 0.1% | 16.2% | 16.2% | 2.5 | 2.1 |

| | | | | | | |
|---|---|---|---|---|---|---|
| 21 | Upper Chincoteague Bay | 15.0% | 2.4% | 17.4% | 0.9 | 0.7 |
| 22 | Assateague Island-Atlantic Ocean | 0.0% | 20.2% | 20.2% | 16.0 | 12.8 |
| 23 | Back River-Frontal Chesapeake Bay | 1.7% | 12.1% | 13.8% | 3.1 | 2.7 |
| 25 | Fairlee Creek-Frontal Chesapeake Bay | 11.8% | 5.7% | 17.5% | 2.6 | 2.1 |
| 27 | Patapsco River-Frontal Chesapeake Bay | 0.7% | 18.0% | 18.7% | 5.0 | 4.0 |
| 28 | Chester River | 16.0% | 3.2% | 19.2% | 1.7 | 1.4 |
| 29 | Western Branch Patuxent River | 3.9% | 0.1% | 4.0% | 1.6 | 1.6 |
| 30 | Zekiah Swamp Run | 16.3% | 0.2% | 16.5% | 0.8 | 0.7 |
| 31 | Transquaking River | 18.1% | 0.8% | 18.9% | 1.7 | 1.4 |
| 32 | Blackwater River | 10.8% | 1.1% | 11.9% | 0.9 | 0.8 |
| 33 | Lower Nanticoke River | 12.2% | 1.0% | 13.2% | 0.8 | 0.7 |
| 34 | Wicomico River | 13.4% | 2.0% | 15.4% | 1.0 | 0.8 |
| 35 | Assawoman Bay | 8.3% | 23.0% | 31.3% | 1.8 | 1.2 |
| 36 | Lower Chincoteague Bay | 3.0% | 4.9% | 7.8% | 0.6 | 0.6 |
| 37 | Metompkin Bay-Burtons Bay | 8.5% | 0.7% | 9.2% | 0.3 | 0.2 |
| 38 | Machipongo River-Hog Island Bay | 12.4% | 1.3% | 13.7% | 0.4 | 0.3 |
| 39 | Magothy Bay-Cobb Bay | 1.9% | 0.4% | 2.3% | 0.1 | 0.1 |
| 40 | Parramore Island-Atlantic Ocean | 0.0% | 0.0% | 0.0% | 2.1 | 2.1 |
| 41 | Manokin River-Frontal Tangier Sound | 23.8% | 2.3% | 26.0% | 0.9 | 0.6 |
| 42 | Upper Tangier Sound | 2.3% | 7.6% | 9.9% | 0.1 | 0.1 |
| 43 | Potomac Creek-Potomac River | 1.4% | 0.8% | 2.2% | 1.6 | 1.6 |
| 44 | Gunpowder River-Frontal Chesapeake Bay | 1.5% | 3.4% | 4.9% | 1.5 | 1.4 |
| 45 | Magothy River-Frontal Chesapeake Bay | 1.1% | 6.3% | 7.4% | 5.6 | 5.2 |
| 46 | Severn River-Frontal Chesapeake Bay | 1.7% | 12.6% | 14.3% | 4.9 | 4.2 |
| 47 | Herring Bay-Frontal Chesapeake Bay | 10.9% | 6.1% | 17.1% | 3.0 | 2.5 |
| 48 | Huntington Creek-Choptank River | 12.0% | 1.1% | 13.1% | 0.7 | 0.6 |
| 49 | Little Choptank River | 27.5% | 2.5% | 30.0% | 5.5 | 3.8 |
| 50 | Wicomico River-Frontal Potomac River | 9.5% | 2.5% | 12.0% | 1.0 | 0.9 |
| 51 | Choptank River-Frontal Chesapeake Bay | 34.1% | 3.7% | 37.8% | 3.9 | 2.4 |

| | | | | | | |
|---|---|---|---|---|---|---|
| 52 | Honga River-Frontal Chesapeake Bay | 7.2% | 2.7% | 9.9% | 0.9 | 0.8 |
| 53 | Watts Creek-Choptank River | 1.2% | 0.5% | 1.7% | 2.0 | 2.0 |
| 54 | Saint Clements Bay-Frontal Potomac River | 7.1% | 3.7% | 10.8% | 2.8 | 2.5 |
| 55 | Saint Marys River-Frontal Potomac River | 10.4% | 3.0% | 13.3% | 3.7 | 3.2 |
| 56 | Nomini Creek-Frontal Potomac River | 1.8% | 1.6% | 3.4% | 2.6 | 2.5 |
| 57 | Occoquan River-Potomac River | 0.5% | 1.9% | 2.4% | 7.0 | 6.9 |
| 58 | Upper Machodoc Creek-Frontal Potomac River | 0.5% | 1.0% | 1.5% | 1.3 | 1.3 |
| 59 | Lynnhaven River-Frontal Chesapeake Bay | 0.0% | 9.2% | 9.2% | 3.4 | 3.1 |
| 60 | Rudee Inlet-Atlantic Ocean | 0.0% | 5.1% | 5.1% | 2.8 | 2.7 |
| 61 | Upper Nanticoke River | 2.9% | 0.3% | 3.3% | 106.9 | 103.4 |
| 63 | Lawnes Creek-James River | 0.0% | 1.4% | 1.4% | 1.1 | 1.1 |
| 65 | Patapsco River | 0.8% | 1.8% | 2.6% | 2.7 | 2.6 |
| 66 | Eastern Bay | 18.0% | 4.1% | 22.1% | 2.4 | 1.8 |
| 68 | South River-Chesapeake Bay | 1.1% | 8.9% | 9.9% | 3.4 | 3.1 |
| 69 | Tuckahoe Creek | 2.9% | 0.2% | 3.1% | 13.0 | 12.6 |
| 70 | Upper Patuxent River | 5.5% | 0.2% | 5.7% | 2.6 | 2.5 |
| 71 | Middle Patuxent River | 21.5% | 0.3% | 21.8% | 0.6 | 0.5 |
| 72 | Lower Patuxent River | 21.2% | 4.6% | 25.8% | 2.0 | 1.5 |
| 73 | Quantico Creek-Potomac River | 0.6% | 0.9% | 1.5% | 1.5 | 1.5 |
| 74 | Sassafras River | 5.8% | 2.6% | 8.4% | 1.0 | 0.9 |
| 75 | Marshyhope Creek | 1.7% | 0.5% | 2.2% | 188.6 | 184.4 |
| 76 | Elk River | 5.8% | 2.9% | 8.7% | 1.8 | 1.6 |
| 77 | Lower Pamunkey River | 0.4% | 0.3% | 0.8% | 1.1 | 1.1 |
| 78 | Upper York River | 3.7% | 0.8% | 4.5% | 0.6 | 0.6 |
| 79 | Lower York River | 2.8% | 1.9% | 4.7% | 1.1 | 1.1 |
| 80 | Occupacia Creek-Rappahannock River | 8.8% | 0.2% | 9.0% | 1.4 | 1.2 |
| 81 | Cat Point Creek-Rappahannock River | 5.6% | 1.0% | 6.6% | 0.8 | 0.8 |
| 82 | Totuskey Creek-Rappahannock River | 1.0% | 0.8% | 1.7% | 1.2 | 1.2 |
| 83 | Lancaster Creek-Rappahannock River | 3.6% | 1.2% | 4.8% | 1.5 | 1.4 |
| 84 | Corrotoman River-Rappahannock River | 0.6% | 2.5% | 3.1% | 2.6 | 2.6 |

| | | | | | | |
|---|---|---|---|---|---|---|
| 85 | Garnetts Creek-Mattaponi River | 0.4% | 0.4% | 0.8% | 1.3 | 1.3 |

991

992

993

Supp. Table 7: Percentage of forest and forested wetland land use within predicted marsh migration area for 1.0 m of sea level rise (SLR) for each HUC watershed. Adjusted 1:1 has the forest and forested wetland land use removed from the marsh migration area when calculating the resilience index. Please note that watersheds 19 and 23 have the same name – this is not a mistake, those are the names from the original source data. Instead we differentiate them by their unique HUC ID numbers. For the location of each watershed, see Supp. Figure 1.

994

995

996

997

| HUC ID# | Name | Forest + Forested Wetland Land Use | Original 1:1 | Adjusted 1:1 |
|---|---|---|---|---|
| 0 | Northwest River | 17.889 | 17.9 | 1.35 |
| 1 | North Landing River | 67.648 | 6.3 | 0.76 |
| 2 | Currituck Sound | 36.229 | 2.3 | 0.98 |
| 3 | Nansemond River | 8.183 | 0.7 | 0.21 |
| 4 | Powhatan Creek-James River | 7.758 | 70.3 | 19.38 |
| 5 | Pagan River-James River | 16.270 | 0.9 | 0.24 |
| 6 | Hampton Roads | 1.185 | 3.1 | 2.29 |
| 7 | Dividing Creek-Pocomoke River | 34.730 | 6.4 | 1.16 |
| 8 | Lower Tangier Sound | 3.701 | 0.4 | 0.34 |
| 9 | Marumsco Creek-Pocomoke Sound | 25.201 | 1.1 | 0.62 |
| 10 | Deep Creek-Pocomoke Sound | 9.177 | 0.7 | 0.36 |
| 11 | Nanjemoy Creek-Potomac River | 6.248 | 1.0 | 0.41 |
| 12 | Great Wicomico River-Frontal Chesapeake Bay | 10.092 | 4.9 | 1.70 |
| 13 | Messongo Creek-Frontal Pocomoke Sound | 20.378 | 1.0 | 0.48 |
| 14 | Piankatank River-Frontal Chesapeake Bay | 6.300 | 3.6 | 1.74 |
| 15 | Mobjack Bay-Frontal Chesapeke Bay | 44.495 | 2.6 | 0.90 |
| 16 | Pungoteague Creek-Frontal Chesapeake Bay | 19.699 | 2.5 | 1.03 |
| 17 | Cherrystone Inlet-Frontal Chesapeake Bay | 4.395 | 2.4 | 1.12 |

| | | | | |
|---|---|---|---|---|
| 18 | Pitts Creek-Pocomoke River | 5.691 | 1.6 | 0.95 |
| 19 | Back River-Frontal Chesapeake Bay | 14.209 | 1.2 | 0.72 |
| 20 | Elizabeth River | 10.016 | 2.5 | 1.59 |
| 21 | Upper Chincoteague Bay | 14.020 | 0.9 | 0.45 |
| 22 | Assateague Island-Atlantic Ocean | 0.412 | 16.0 | 14.30 |
| 23 | Back River-Frontal Chesapeake Bay | 2.053 | 3.1 | 2.04 |
| 25 | Fairlee Creek-Frontal Chesapeake Bay | 4.010 | 2.6 | 1.63 |
| 27 | Patapsco River-Frontal Chesapeake Bay | 1.873 | 5.0 | 3.78 |
| 28 | Chester River | 12.220 | 1.7 | 0.88 |
| 29 | Western Branch Patuxent River | 0.729 | 1.6 | 0.72 |
| 30 | Zekiah Swamp Run | 1.291 | 0.8 | 0.27 |
| 31 | Transquaking River | 26.333 | 1.7 | 0.79 |
| 32 | Blackwater River | 49.137 | 0.9 | 0.56 |
| 33 | Lower Nanticoke River | 18.795 | 0.8 | 0.46 |
| 34 | Wicomico River | 24.921 | 1.0 | 0.48 |
| 35 | Assawoman Bay | 5.974 | 1.8 | 1.23 |
| 36 | Lower Chincoteague Bay | 18.309 | 0.6 | 0.35 |
| 37 | Metompkin Bay-Burtons Bay | 7.353 | 0.3 | 0.16 |
| 38 | Machipongo River-Hog Island Bay | 19.268 | 0.4 | 0.15 |
| 39 | Magothy Bay-Cobb Bay | 5.478 | 0.1 | 0.06 |
| 40 | Parramore Island-Atlantic Ocean | 0.097 | 2.1 | 2.10 |
| 41 | Manokin River-Frontal Tangier Sound | 27.412 | 0.9 | 0.50 |
| 42 | Upper Tangier Sound | 1.189 | 0.1 | 0.10 |
| 43 | Potomac Creek-Potomac River | 3.837 | 1.6 | 0.51 |
| 44 | Gunpowder River-Frontal Chesapeake Bay | 4.233 | 1.5 | 0.95 |
| 45 | Magothy River-Frontal Chesapeake Bay | 0.907 | 5.6 | 3.58 |
| 46 | Severn River-Frontal Chesapeake Bay | 1.727 | 4.9 | 3.03 |
| 47 | Herring Bay-Frontal Chesapeake Bay | 7.924 | 3.0 | 1.84 |
| 48 | Huntington Creek-Choptank River | 3.810 | 0.7 | 0.35 |
| 49 | Little Choptank River | 47.444 | 5.5 | 2.76 |

| | | | | |
|---|---|---|---|---|
| 50 | Wicomico River-Frontal Potomac River | 2.705 | 1.0 | 0.52 |
| 51 | Choptank River-Frontal Chesapeake Bay | 16.997 | 3.9 | 2.60 |
| 52 | Honga River-Frontal Chesapeake Bay | 25.901 | 0.9 | 0.51 |
| 53 | Watts Creek-Choptank River | 3.344 | 2.0 | 0.50 |
| 54 | Saint Clements Bay-Frontal Potomac River | 3.366 | 2.8 | 1.73 |
| 55 | Saint Marys River-Frontal Potomac River | 5.854 | 3.7 | 1.95 |
| 56 | Nomini Creek-Frontal Potomac River | 8.163 | 2.6 | 0.89 |
| 57 | Occoquan River-Potomac River | 3.921 | 7.0 | 2.08 |
| 58 | Upper Machodoc Creek-Frontal Potomac River | 3.808 | 1.3 | 0.33 |
| 59 | Lynnhaven River-Frontal Chesapeake Bay | 6.846 | 3.4 | 1.69 |
| 60 | Rudee Inlet-Atlantic Ocean | 0.182 | 2.8 | 1.92 |
| 61 | Upper Nanticoke River | 4.644 | 106.9 | 10.02 |
| 63 | Lawnes Creek-James River | 8.074 | 1.1 | 0.26 |
| 65 | Patapsco River | 0.498 | 2.7 | 1.72 |
| 66 | Eastern Bay | 10.426 | 2.4 | 1.34 |
| 68 | South River-Chesapeake Bay | 1.181 | 3.4 | 2.04 |
| 69 | Tuckahoe Creek | 1.975 | 13.0 | 4.09 |
| 70 | Upper Patuxent River | 2.338 | 2.6 | 1.07 |
| 71 | Middle Patuxent River | 3.832 | 0.6 | 0.32 |
| 72 | Lower Patuxent River | 3.491 | 2.0 | 1.32 |
| 73 | Quantico Creek-Potomac River | 3.976 | 1.5 | 0.51 |
| 74 | Sassafras River | 1.804 | 1.0 | 0.44 |
| 75 | Marshyhope Creek | 5.059 | 188.6 | 26.19 |
| 76 | Elk River | 3.411 | 1.8 | 0.93 |
| 77 | Lower Pamunkey River | 11.069 | 1.1 | 0.63 |
| 78 | Upper York River | 7.519 | 0.6 | 0.26 |
| 79 | Lower York River | 7.405 | 1.1 | 0.42 |
| 80 | Occupacia Creek-Rappahannock River | 7.979 | 1.4 | 0.50 |
| 81 | Cat Point Creek-Rappahannock River | 5.407 | 0.8 | 0.49 |
| 82 | Totuskey Creek-Rappahannock River | 4.088 | 1.2 | 0.54 |
| 83 | Lancaster Creek-Rappahannock River | 4.781 | 1.5 | 0.64 |

| | | | | |
|---|---|---|---|---|
| 84 | Corrotoman River-Rappahannock River | 5.549 | 2.6 | 0.86 |
| 85 | Garnetts Creek-Mattaponi River | 5.304 | 1.3 | 0.78 |

998